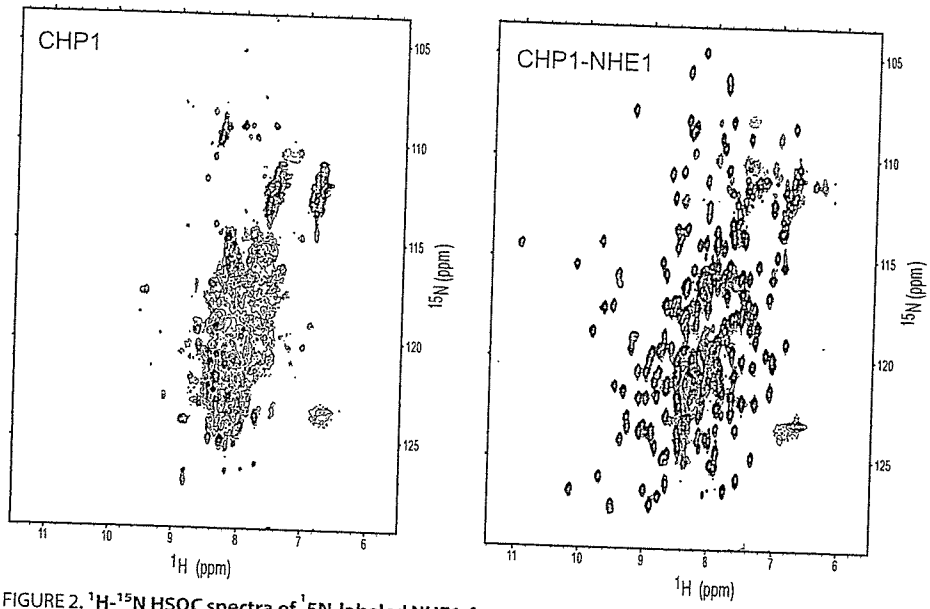

FIGURE 2. **^{1}H-^{15}N HSQC spectra of ^{15}N-labeled NHE1-free CHP1 (*left image*) and ^{15}N-labeled NHE1-(503–545)-CHP1 complex (*right image*).** These spectra were obtained with 0.3 mM samples at pH 6.9 and 37 °C recorded on the AVANCE 500.

TABLE 1

Structural statistics for NHE1-CHP1

These statistics represent an ensemble comprising 20 of the lowest energy structures obtained from 150 starting structures. Structure calculations were performed using XPLOR-NIH version 2.9.6.

Total number of distance constraints	4242
Long range ($\|i-j\|>4$)	589 (inter: 134)
Middle range ($\|i-j\|=2,3,4$)	874
Short range ($\|i-j\|=1$)	1038
Intraresidue	1521
Hydrogen bond constraints (including Ca^{2+} coordination restraints)	110 × 2
Dihedral constraints	
ϕ, φ	105, 105
$\chi 1$	17
r.m.s. deviation from experimental constraints[a]	
Distance (Å)	$0.0288 \pm 7 \times 10^{-4}$
Angle (°)	$0.44 \pm 3 \times 10^{-2}$
r.m.s. deviation from idealized covalent geometry	
Bonds (Å)	$0.00248 \pm 6 \times 10^{-5}$
Angles (°)	$0.360 \pm 6 \times 10^{-3}$
Impropers (°)	$0.31 \pm 1 \times 10^{-2}$
XPLOR energy terms (kcal/mol)[b]	
E_{bond}	23 ± 1
E_{angle}	138 ± 5
E_{imp}	28 ± 2
$E_{vdw(LJ)}$	$-6.6 \times 10^{2} \pm 0.2 \times 10^{2}$
PROCHECK Ramachandran plot (185–254)	
Residues in most favored regions (%)	78.6
Residues in additional allowed regions (%)	18.1
Residues in generously allowed regions (%)	2.9
Residues in disallowed regions (%)	0.4
r.m.s. deviation of mean structure derived from 30 calculated structures	
Backbone (10–92, 108–192, 516–538) (Å)	0.53
All heavy (10–92, 108–192, 516–538) (Å)	1.15

[a] None of these structures exhibited distance violations >0.5 or dihedral angle violations >5°.

[b] $E_{vdw(LJ)}$ represents the Lennard-Jones energy of the XPLOR energy terms.

complexed with NHE1 is well dispersed with favorable line shapes (Fig. 2), suggesting that the complex essentially adopts an ordered monomeric structure in solution.

Our target complex was ~27 kDa in size, assuming a 1:1 complex of CHP1 (22 kDa) and NHE1 (5 kDa). This represented a relatively large molecular weight in terms of conventional NMR studies. Consequently utilization of triple labeling (^{2}H, ^{13}C, and ^{15}N) and the recently developed computational methodology, CANDID, was extremely helpful in the structure determination. Sequential backbone assignments and most side-chain assignments were obtained from a 60% ^{2}H/^{15}N/^{13}C-labeled sample using standard triple resonance experiments. Missing ^{1}H resonances were supplemented using heteronuclear three-dimensional NOESY experiments with ^{15}N/^{13}C-labeled samples. Resonance assignments of methyl groups were carefully confirmed in a stereospecific manner using two-dimensional Constant Time HSQC spectra recorded for a 15% randomly enriched ^{13}C sample. Methyl groups for 18 of 24 leucines and nine of 11 valines were stereospecifically assigned. Aromatic ring proton assignments, essential for delineating hydrophobic core and protein-protein interactions, were obtained using two-dimensional TOCSY, two-dimensional NOESY, two-dimensional HCCH(arom) TOCSY, and three-dimensional ^{13}C(arom)-edited ^{15}N-separated NOESY experiments.

NMR spectra including the three-dimensional ^{13}C-edited NOESY spectrum used to monitor inter/intramolecular ^{1}H-^{1}H NOEs were of adequate quality to pursue a structural determination of the NHE1-CHP1 complex. Use of partial deuteration and the almost complete resonance assignment of methyl groups forming the hydrophobic core facilitated an initial determination of the overall protein fold. A high resolution structure was subsequently obtained using CANDID for automated assignments, which included the use of ambiguous NOEs from ^{15}N- and ^{13}C-edited NOESY experiments recorded for ^{15}N- or ^{15}N/^{13}C-labeled protein samples. An iterative approach was used for assigning NOEs in addition to the manually assigned unambiguous NOEs. The solution structure of the CHP1-NHE1 complex was determined from a total of over 4000 NMR-derived restraints, including 134 intermolecular distance restraints (Table 1). The ensemble of 20 structures in excellent agreement with a large body of experimental data were well defined (Fig. 3*A*). The r.m.s. deviations of backbone and heavy atoms over residues 518–537 of NHE1 and residues 10–92 and 108–193 of CHP1 were 0.53 and 1.15 Å, respectively. Of the NMR structures determined, the one with the smallest total energy was selected as representative for further discussion. The complex is predominantly α-helical, and the CHP1 helices constitute a cleft. A helix of the cytoplasmic region of NHE1 associates with CHP1 in 1:1 stoichiometry via the cleft (Fig. 3, *A* and *B*).

Structure of NHE1—NHE1 forms a five-turn amphipathic helix composed of residues 518–537. Orientation of the NHE1 helix is well defined relative to CHP1, consistent with the large

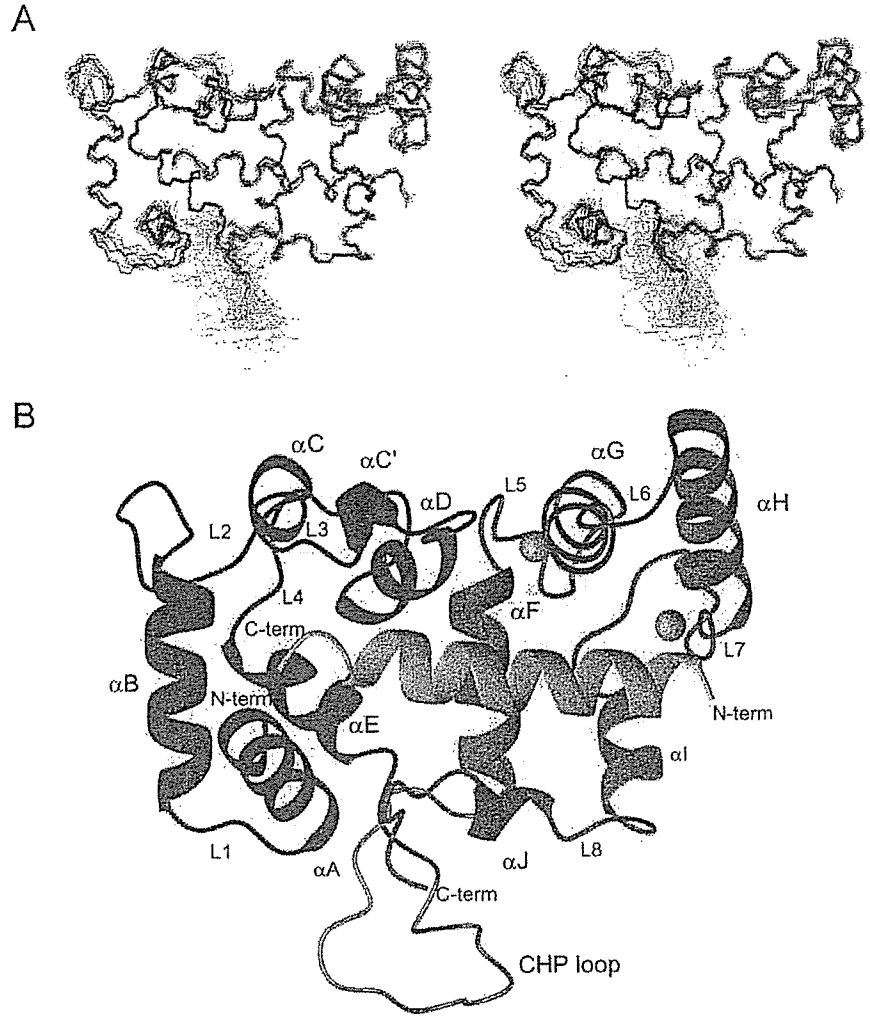

FIGURE 3. **Solution structure of the NHE1-CHP1 complex.** *A*, stereoview of the backbone superpositions of the final 20 simulated annealing structures of the NHE1-CHP1 complex. *B*, ribbon drawing of the representative NHE1-CHP1 structure complex. *A* and *B*, residues 517–538 of NHE1 and 10–192 of CHP1 are shown. The N- and C-terminal domains of CHP1 are colored in *blue* and *magenta*, respectively, and the CHP loop is colored in *gray*. NHE1 is shown in *green*. Ca^{2+} ions are shown by *gold spheres*.

number of intermolecular NOEs detected between CHP1 and NHE1 (Table 1 and Fig. 3*A*). The N-terminal half of the helix (residues 518–530) binds to the C-terminal domain of CHP1, and the C-terminal half of the helix (residues 531–537) binds to the N-terminal domain of CHP1 (Fig. 4*A*). Side-chain conformations of the helix are also well defined particularly for apolar residues that make extensive contacts with CHP1. For example, NMR spin-echo difference $^3J_{NC\gamma}$ and $^3J_{C'C\gamma}$ experiments, which bring about $\chi 1$ rotamer information of aromatic side chain, showed that the His-523 and Phe-526 adopted *g*+ and *t* conformations, respectively. The helix exhibits amphipathic character in which the bulky hydrophobic residues Ile-518, Ile-522, His-523, Phe-526, Leu-527, Leu-530, Leu-531, Ile-534, and Ile-537 are clearly confined to one side, and hydrophilic residues are exposed at the other side (Fig. 4*B*). The hydrophobic residues form a continuous apolar surface (Fig. 4*B*). The main-chain and side-chain conformations of residues preceding and following the helix, residues 503–517 and 538–545, respectively, are poorly defined in the NMR structure because of the absence of medium and long range NOEs involving these regions. The narrow resonance linewidths, chemical shift index, and steady state $\{^1H\}$-^{15}N heteronuclear NOE suggest that these regions are unstructured in the complex.

Structure of CHP1—CHP1 is composed of 10 α-helices and a long loop folded into two globular regions representing the N- and C-terminal domains (Fig. 3*B*). The secondary structure consists of αA (residues 11–22), αB (residues 26–37), αC (residues 48–51), αD (residues 64–70), αE (residues 80–88), αF (residues 111–122), αG (residues 132–143), αH (residues 149–162), αI (residues 174–180), and αJ (residues 185–188) (Figs. 1*B* and 3*B*). The N-terminal domain consists of ancestral EF-hands, EF-1 and EF-2, that do not bind calcium under physiological conditions. The EF-1 hand includes helix αB, loop L2, and helix αC followed by loop L3 to the second EF-hand that includes helix αD, loop L4, and helix αE (Figs. 1*B* and 3*B*). A long loop region consisting of residues 93–110 connects the N- and C-terminal domains. Because this characteristic long insertion is not found in calcineurin B (Figs. 1*B* and 3, *A* and *B*), we refer to this long loop as the CHP loop. The absence of medium and long range NOEs, a chemical shift index, and $\{^1H\}$-^{15}N heteronuclear NOE value indicate that this region is flexible in solution. The first EF-hand in the C-terminal domain includes helix αF, loop L5, and helix αG followed by loop L6 and the second EF-hand that consists of helix αH, loop L7, and helix αI (Figs. 1*B* and 3*B*).

The four CHP1 EF-hands form a deep hydrophobic pocket, which constitutes the interaction surface for the NHE1 amphipathic α-helix. CHP1 binds to the apolar side of NHE1 with the four EF-hands through a side-by-side manner (Fig. 4*A*). This contrasts with the well known canonical CaM-target binding mode that represents a wrap-around manner in which two pairs of EF-hands bind to the target IQ motif helix on opposite sides to each other (43, 44).

Although there is modest sequence similarity between CHP1 and CaM, it should be noted that the latter interacts with a large number of proteins with various interaction modes including canonical 1:1 binding and non-canonical 1:1, 1:2, and 2:2 binding (43, 44). It has been suggested that the observed binding versatility of CaM could be derived from the variable positioning of the two domains, linked by a flexible linker, that can

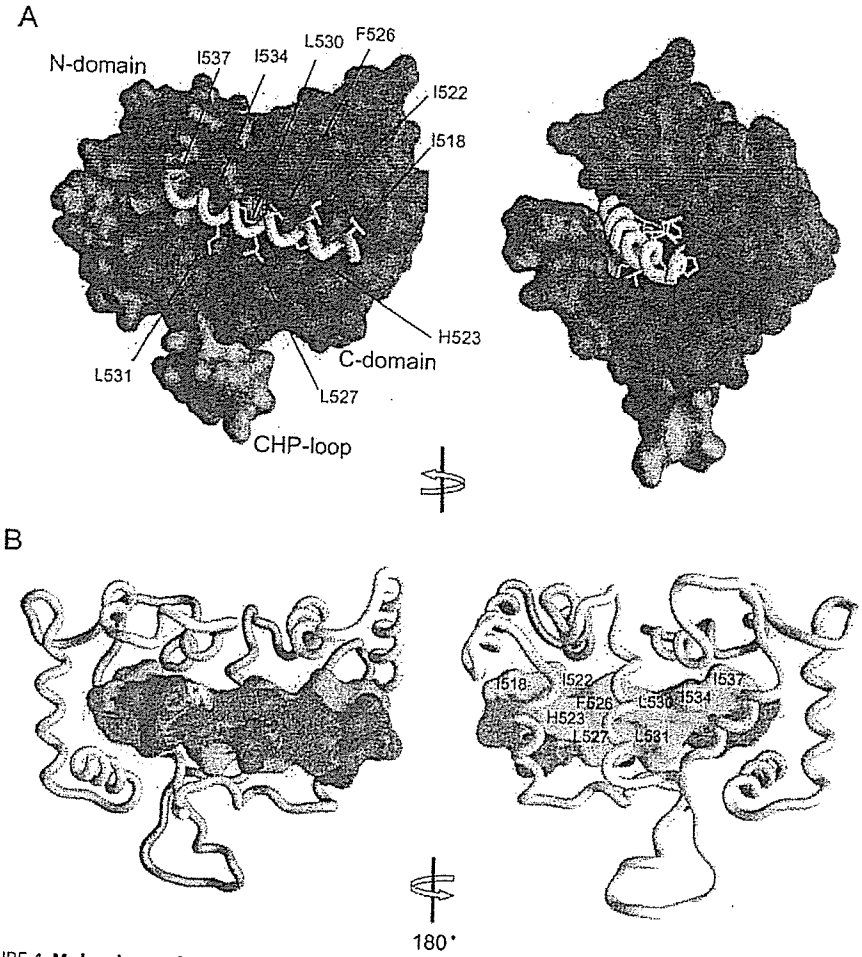

FIGURE 4. **Molecular surface of the NHE1-CHP1 complex.** *A*, molecular surface of CHP1 and backbone *tube* representation of NHE1 with *yellow stick* that shows the hydrophobic side chains. The N- and C-terminal domains of CHP1 are colored in *blue* and *magenta*, respectively. *B*, molecular surface of NHE1 and backbone *tube* representation of CHP1. Hydrophobic, acidic, and polar residues are colored in *yellow*, *red*, and *blue*, respectively.

accommodate different targets. Although target multiplicity has been reported in the case of CHP1, it seems to possess more limited binding modes than CaM. One notable feature of CHP1 that illustrates its difference to CaM has to do with the interdomain interaction. This interaction restricts domain orientation, a phenomenon absent in CaM. In our CHP1 structure, residue Leu-62 of the N-terminal domain participates in a hydrophobic interaction with residues Val-138 and Met-141 of the C-terminal domain, and residue Ala-69 of the N-terminal domain interacts with residue Leu-122 of the C-terminal domain. A side-by-side interaction mediated by four EF-hands has also been reported to take place with voltage-gated potassium channel (Kv)-interacting protein (KChIP) (45) and with CNA-CNB (46, 47) (Fig. 5*A*).

The atomic r.m.s. difference of well fitted parts between CHP1 complexed with NHE1 and CNB complexed with CNA (Protein Data Bank code 1AUI) is 2.7 Å, indicating that the fit is not very good, although the topology is identical with a high Z-score of 11.8 from a distance matrix alignment (DALI) search. The r.m.s. deviation value improves to 1.7 Å when only the N-terminal domains are superimposed, and it is 1.8 Å when only the C-terminal domains are superimposed. This indicates that the higher r.m.s. deviation for both domains originates from an interdomain swiveling between NHE1-CHP1 and CNA-CNB, although both proteins bind cognate targets in a side-by-side manner. Similarly domain swiveling was observed between NHE1-bound and NHE-free CHP1. Swiveling of the N- and C-terminal domains could create a binding surface for cognate targets.

Comparison with Other EF-hands—It is interesting to note that both EF-1 and EF-2 adopt an open conformation in NHE1-bound CHP1 without Ca^{2+}. This is especially evident when comparing the angles between the EF-hand helices. In Fig. 5*B*, a graphical view of the interhelical angles between the first and second helices of EF-1 and EF-2 of apoCaM (a typical closed conformation), Ca^{2+}-CaM (a typical open conformation, CNB), KChIP1, NHE1-bound CHP1, and NHE1-free CHP1 is displayed using a vector geometry mapping method (48, 49). The first helices of the EF-hands are superimposed along the *z* axis, and the spatial localization of the second helices are shown as a *cylinder*. This indicates that both EF-1 and EF-2 of NHE1-bound CHP1 adopt an open conformation, whereas EF-1 and EF-2 of NHE1-free CHP1 adopt an open and semiopen conformation, respectively (Fig. 5*B* and supporting information S1). This implies that EF-1 and EF-2 adopt a constitutively open conformation. However, it should be noted that the hydrophobic cleft of the N-terminal domain of free CHP1, as revealed by the crystal structure, is plugged by additional linker residues (Leu-Ala-Ala-Ala-Leu-Glu-His) (23) derived from the expression vector, partly mimicking the NHE1 helix (Fig. 5*A*). Binding of the vector-derived linker might have facilitated adoption of the open and semiopen conformations of EF-1 and EF-2, respectively. Therefore, the possibility of a "closed to open" conformational transition of EF-1 and EF-2 remains to be evaluated.

The binding of EF-hands in an open conformation without Ca^{2+} to target molecules has been found following crystal structure investigations of a Kv-KChIP1 in which the Kv fragment is covalently linked to the C terminus of KChIP1 (45). In this case, the Kv fragment binds to EF-1 and EF-2 of the N-terminal domain of KChIP1 through hydrophobic interactions (Fig. 5*A*). Of particular note, KChIP1 forms a dimer utilizing the surface formed by the Kv peptides and helix 10 of the C-terminal domain of KChIP1 in contrast to NHE1-CHP1, which exists as a monomer (Fig. 5*C*). The interhelix angles of EF-1 and EF-2

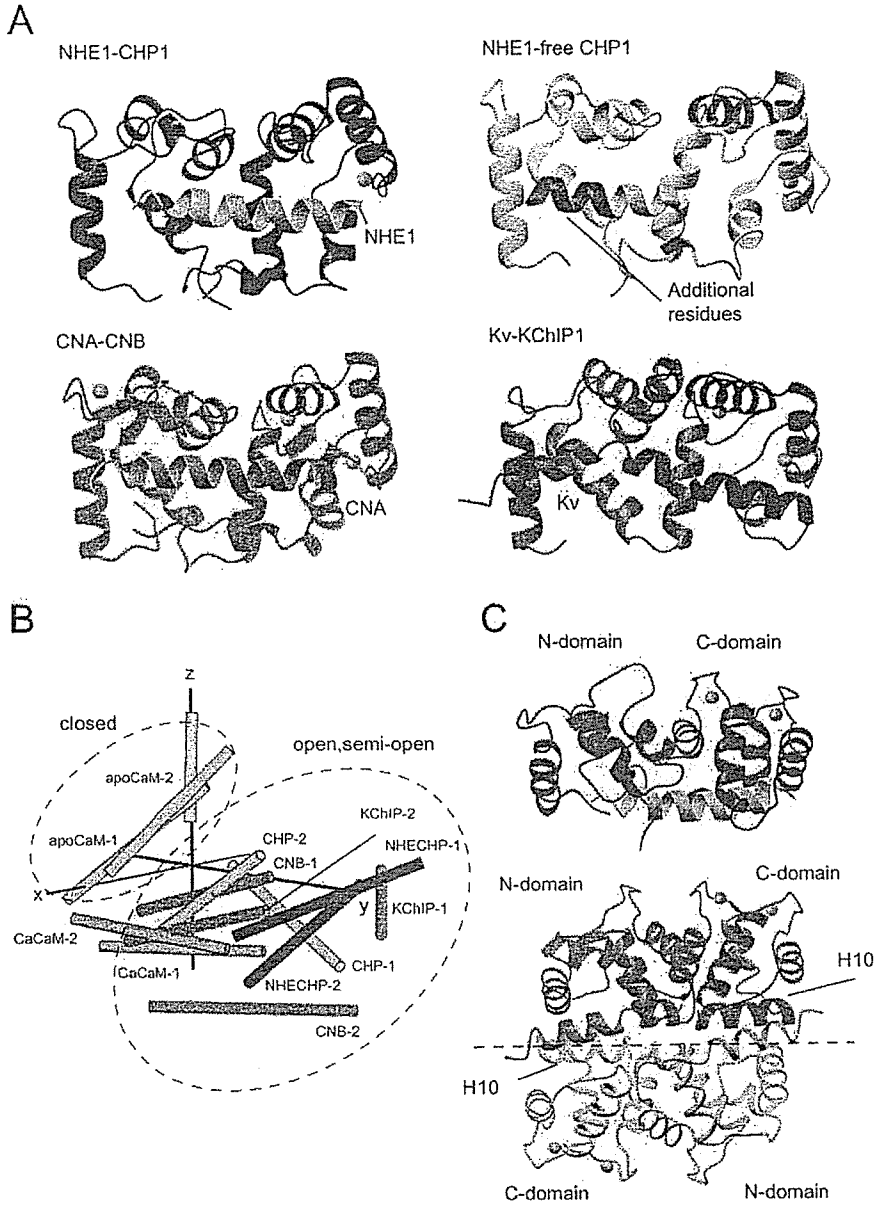

FIGURE 5. **Structure comparisons.** *A*, ribbon representation of NHE1-CHP1, rat NHE1-free CHP1 (2CT9) in which additional residues from the expression vector interacting with the N-terminal domain (LAAALEH) are depicted in *magenta*, CNA-CNB (1AUI), and Kv-KChIP1 (1S6C). Protein Data Bank entries are shown in parentheses. *B*, vector geometry mapping of EF-1 and EF-2 apocalmodulin, Ca^{2+}-calmodulin, calcineurin B, Kv-KChIP1, NHE1-bound CHP1, and NHE1-free CHP1 are denoted as *"apoCaM," "CaCaM," "CNB," "KChIP," "NHECHP,"* and *"CHP,"* respectively. *Hyphenated numbers 1* and *2* denote EF-1 and EF-2, respectively, for each protein. *C*, comparison of the KChIP1 dimer and CHP1 structures colored in *brown* and *blue*, respectively. Bound Kv and NHE1 are colored in *pink* and *green*, respectively. The dimer interface of KChIP1 is shown as a *dashed line*, and one molecule of the dimer is shown in *light colors*. KChIP1 and CHP1 are depicted in the same orientation. In *A* and *C*, the N- and C-terminal regions, αA, and the CHP loop of CHP1 are not shown in the comparison for reasons of clarity.

are 82° and 72°, respectively (supporting information S1), which are slightly larger than those of CHP1. A dimeric interaction in addition to binding of the Kv fragment may contribute to broadening of the cleft constituted by EF-1 and EF-2.

CHP1 shares 18% sequence identity with KChIP1, and the folding topology is almost identical (Fig. 5*A*). However, the target recognition mechanism differs from that of KChIP1 as judged from the determined structures. KChIP1 belongs to the extensively studied NCS1 family, which act as important regulators of various functions among certain higher eukaryotes (50). We propose that the NHE1-CHP1 interaction represents a novel binding mode utilized throughout the four-EF-hand proteins, which constitute a distinct subfamily to the NCS1 family. Furthermore detailed comparison of the binding mode of CHP1 and CNB will be presented below.

The CHP1-NHE1 Interface—The protein-protein interface consists of an extensive hydrophobic concave CHP1 undersurface and an apolar NHE1 surface. The concave undersurface spans both the N- and C-terminal domains of CHP1. The total surface area buried at the interface is 2338 $Å^2$, slightly smaller than the value of 2625 $Å^2$ for the interface between CNA and CNB (Protein Data Bank code 1AUI). Approximately more than 90% of the total buried surface area between NHE1 and CHP1 is hydrophobic, similar to the complexed structure of CNA and CNB.

The interface formed between NHE1 and CHP1 includes methyl-containing and aromatic hydrophobic residues. The residues of the N-terminal domain of CHP1, Ala-69, Phe-90, Ile-66, Thr-86, Leu-87, Phe-35, and Leu-54, comprise a hydrophobic cleft that interacts with the apolar surface formed by the side chains of NHE1 residues Leu-530, Ile-534, and Ile-537. Additionally the side chain of NHE1 Leu-531 expands the hydrophobic area interacting with CHP1 Phe-90 (Fig. 6*A*). The C-terminal domain residues of CHP1, Ala-163, Thr-159, Leu-139, Leu-135, Tyr-122, Phe-176, Ile-171, Phe-117, Ala-118, and Leu-121, constitute a continuous hydrophobic cleft that interacts with the N-terminal portion of NHE1 helix residues Ile-518, Ile-522, and Phe-526, which protrude at the apolar side. NHE1 residues Leu-527 and His-523 make additional hydrophobic contact with CHP1 residues Tyr-122, Phe-176, and Val-185 (Fig. 6*A*). These interface-forming hydrophobic residues are well conserved within NHE and CHP isoforms, reflecting the importance of these interactions (Fig. 1*B*). Furthermore the acidic side chain of Asp-528 at the center of NHE1 helix seems to form a salt bridge with the basic side

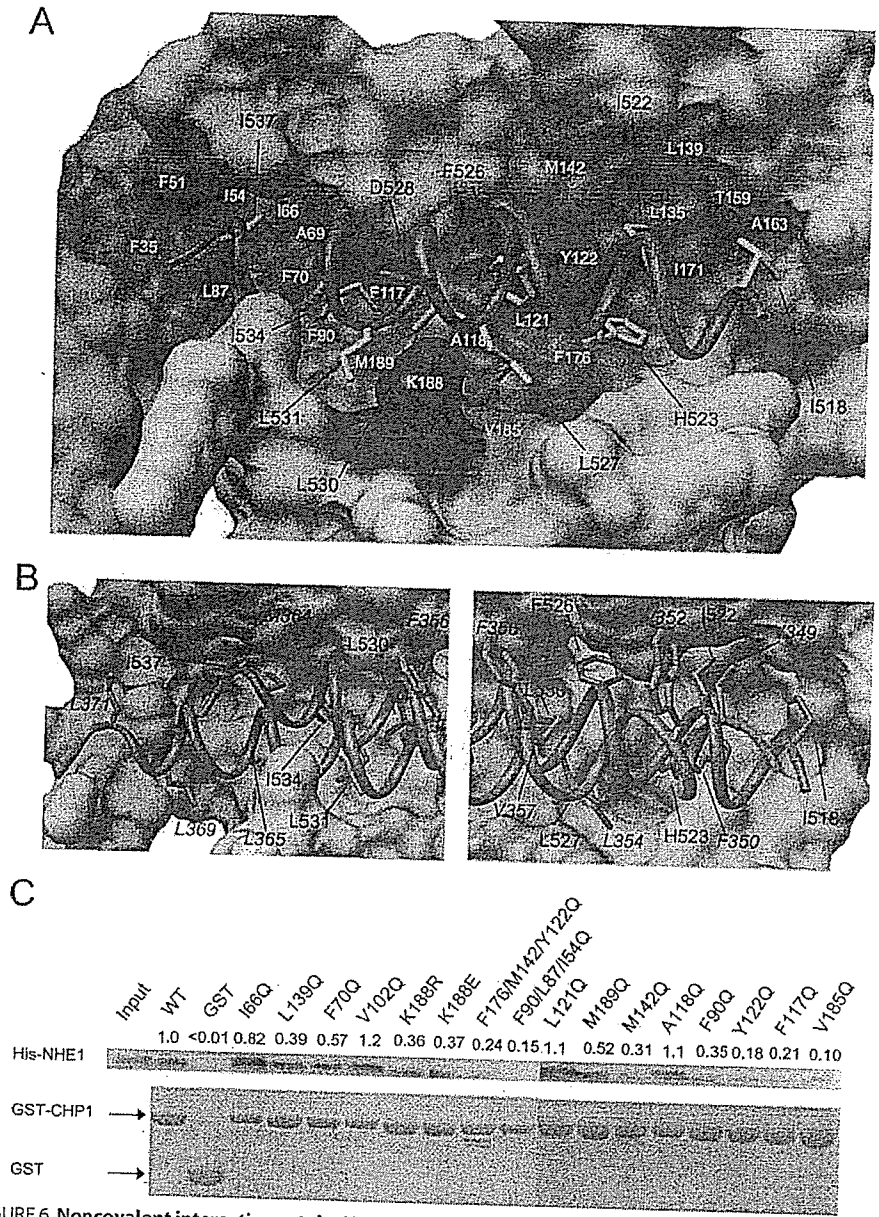

FIGURE 6. **Noncovalent interactions at the NHE1-CHP1 interface and contribution to the overall stability of the complex.** *A*, molecular surface of CHP1 and backbone *tube* representation of NHE1 with *yellow* and *red sticks* that show hydrophobic and acidic side chains, respectively. Hydrophobic and basic surface residues of CHP1 are colored in *orange* and *blue*, respectively. *B*, superposition of NHE1-CHP1 and CAN-CNB (Protein Data Bank code 1AUI). NHE1 and CNA are shown in *green* and *magenta*, respectively, and the molecular surface of only CHP1 is depicted for clarity. Complex-forming hydrophobic residues of NHE1 and CNA are shown as *sticks* and are labeled. CNA residues are represented in *italics*. The *left-hand image* and the *right-hand image* are close-up views of the N- and C-terminal domains. *C*, binding of His-NHE1 peptide to GST-CHP1 mutants in an *in vitro* pulldown assay. Bound peptide was separated via SDS-PAGE, blotted to a membrane, and then visualized using Ni-NTA-conjugated alkaline phosphatase (*top*). The amount of GST-CHP1 mutant used was estimated by Coomassie Blue staining (*bottom*) for calibration. The binding of NHE1 peptide to GST-CHP1 mutants was quantified and expressed as a ratio of binding of wild-type protein at the *top* of the gel images.

chain of CHP1 Lys-188. The presence of this interaction was observed in 10 of the final 20 NMR structures derived using the MONSTER server (51), which identifies interacting residues and assigns the nature of those interactions based on the structure. These residues are also conserved (Figs. 1, *A* and *B*, and 6*A*).

NHE1 binding orientation relative to CHP1 is probably established by surface complementarity that comprises the hydrophobic surfaces of NHE1 and CHP1. NHE1 side chains of Ile-534 and Ile-537 protrude into the shallow cleft made by the CHP1 N-terminal domain. Meanwhile NHE1 aromatic side chains of His-523 and Phe-526 protrude into the deep cleft of the CHP1 C-terminal domain (Fig. 6*A*). This deep cleft allows enough space so that they can interact with the bulky side chains of NHE1. The difference between the shapes of the domains is critical for NHE1 binding orientation.

Notably the shape of the interaction surfaces of NHE1-CHP1 and CNA-CNB differs. The spatial arrangement of NHE1 and CNA residues that contribute to form the interaction surfaces differs for each (Fig. 6*B*). Only Val-349, Phe-350, and Val-357 of CNA are located at equivalent positions to Ile-522, His-523, and Leu-530 of NHE1 unlike other residues. Cleary Trp-352 and Phe-356 of CNA that interact with the roof of the hydrophobic cleft formed by CNB are missing in NHE1. Furthermore the interactions mediated by the C-terminal stretch region of CNA, where Leu-369 and Leu-371 protrude, are absent in NHE1. On the other hand, the corresponding residues to Phe-526 and Ile-518 of NHE1 are absent in CNA.

Consequently the interaction mechanism dominated by hydrophobic interactions through amphipathic helices and four EF-hands is common in both complexes, but their shape differs. This surface complementarity in terms of a knobs-into-hole mode of interaction defines the binding specificity of these proteins, although the folding topology is identical.

Correlation with Mutagenesis Studies—The solution structure of the CHP1-NHE1 complex is essentially consistent with previous mutagenesis studies concerning NHE1. Co-immunoprecipitation experiments showed that the 4Q mutant of NHE1, in which Phe-526, Leu-527, Leu-530, and Leu-531 are substituted with glutamine, displayed no binding to CHP1, whereas the I518Q/I522Q NHE1 double mutant displayed some binding albeit with decreased affinity (3). Our structure determination revealed that Phe-526, Leu-527, Leu-530, and Leu-531 form a hydrophobic core that interacts with the center of the hydrophobic cleft of the C-terminal domain of

CHP1, whereas Ile-518 and Ile-522 interact with the rim of the hydrophobic cleft of the C-terminal domain of CHP1 (Figs. 4*B* and 6*A*). Deletion mutagenesis indicated that NHE1 (residues 510–575) retained binding affinity similar to the wild-type protein, implying that the juxtamembrane region of NHE1 comprising residues 503–509 is unimportant for CHP1 binding (3). These residues were found to be unstructured in the present study and form no direct contact with NHE1.

The binding activity of NHE1 (residues 530–656) lacking the N-terminal segment was found to be completely impaired (3). Our NHE1-CHP1 complex structure shows that an absence of residues preceding Leu-530 results in almost complete loss of interaction between NHE1 and the C-terminal domain of CHP1, whereas the many hydrophobic interactions mediated by NHE1 residues Leu-530, Leu-531, Ile-534, and Ile-537 are retained (Fig. 6*A*). This indicates that interaction of the N-terminal residues of NHE1 and the C-terminal domain of CHP1 is indispensable in maintaining the NHE1-CHP1 complex. Namely this part of the interaction plays a dominant role in NHE1-CHP1 complex formation.

CHP1 was subjected to site-directed mutagenesis in an effort to reveal detailed individual contributions of interfacial residues toward the overall stability of the NHE1-CHP1 complex. We selected three categories of residues in CHP1: 1) residues that comprise the floor of the hydrophobic pocket, Phe-70, Phe-90, Phe-117, Ala-118, Leu-121, Tyr-122, and Met-189; 2) residues forming the rim of the pocket, Ile-66, Leu-139, Met-142, and Val-185; and 3) a residue forming the salt bridge, Lys-188. A noninteracting solvent-exposed residue, Val-102, as the positive control and a triple mutation involving hydrophobic residues Phe-90/Leu-87/Leu-54 and Phe-176/Met-142/Tyr-122 as the negative control were prepared.

Dramatic effects were observed in terms of CHP1 binding to NHE1 with mutations F117Q, Y122Q, and V185Q (Fig. 6*C*). We expected the floor-forming residues located at the bottom of the cleft to be critical for the interaction, but the rim-forming residue Val-185 showed significant reduction similar to the negative control. Based on the solution structure of the NHE1-CHP1 complex, it was appeared that Phe-117, Tyr-122, and Val-185 were confined to the C-terminal domain of CHP1 and were packed against the apolar side of NHE1. This suggests that the C-terminal hydrophobic cleft represents a mutation hot spot, implying that it plays a key role in the NHE1-CHP1 interaction. This result is consistent with the NHE1 deletion result indicating that interaction between the N-terminal segment of NHE1 and the C-terminal domain of CHP1 is dominant. This represents a unique feature of the NHE1-CHP1 interaction.

Although mutation of residues possibly involved in salt bridge formation such as K188E and K188R resulted in a marked decrease in binding interaction, the effect was not strong, and the charge-reversing effect of K188E was unclear. Thus, it appears that although this salt bridge contributes to NHE1-CHP1 complex formation, it is not the main force possibly because this bond is exposed to solvent (Fig. 6*A*), and therefore solvation could weaken the strength of the interaction.

Role of CHP1—NMR investigations of NHE1 complexed with CHP1 revealed that the juxtamembrane region comprising residues 503–517 was unstructured in solution. This region is rich in basic residues with a previous study reporting that NHE1 comprising residues 506–576 bound to PIP_2 *in vitro* (13). In addition, residues 513–520 and 556–564 might represent PIP_2 binding sites (13). Accordingly it is likely that this juxtamembrane region (residues 503–517) following the last transmembrane helix (H12, residues 478–499) is incapable of forming a continuous straight helical structure into the cytoplasm due to interaction with the membrane. Rather the overall structure of NHE1 presumably turns or bends toward the cytoplasmic membrane following a PIP_2-mediated interaction. Assuming that flanking regions of the helix, residues 513–520 and 556–564, attach to the membrane (PIP_2) (13), the helix and CHP1 should be located immediately beneath the cytoplasmic membrane.

Furthermore it has been reported that NHE1 acts as a scaffold protein linked to actin filaments via ezrin-radixin-moesin proteins in addition to possessing function as an ion exchanger (52, 53). Our NMR studies revealed that the cytoplasmic helix-forming residues of NHE1 comprise residues 518–537, which showed little overlap from the previously reported ezrin-radixin-moesin binding region (512–520 and 550–565). This ensures simultaneous binding of NHE1 to CHP1 and ezrin-radixin-moesin proteins.

The juxtamembrane region of NHE1 forms a particular tertiary or quaternary structure that is mediated by interactions with the membrane (PIP_2), CHP1, and ezrin-radixin-moesin proteins. The overall structure of the juxtamembrane region might play an important role in NHE1 activity. The 90% loss in activity following CHP1 depletion might be due to disruption of the structure of the cytoplasmic region of NHE1 around the membrane. In fact, although this represents *in vitro* evidence, the amphipathic helix is disrupted in the absence of CHP1 based on the CD and NMR data (supporting information S2 and S3).

Possible Mode of Regulation—CHP1 deprivation resulted in impaired regulation of NHE1 following external stimuli, implying that CHP1 acts as regulator of NHE1 by involvement in the processing of intracellular signals derived from external stimuli. However, the regulatory mechanism remains unclear. Although it was reported that CHP1 is an *N*-myristoylated protein, CHP1 does not exert myristoyl switching in a Ca^{2+}-dependent manner under normal physiological conditions because EF-3 and EF-4 constitutively bind Ca^{2+} ions where *N*-myristoylation was not required for NHE1 binding, activation, or localization (14).

Of particular note, it was reported that CHP1 is a phosphorylated protein, although the phosphorylation sites were not determined. According to the phosphorylation prediction server NetPhos (54), the CHP1 sequence contains potential phosphorylation sites located at residues Thr-36, Ser-37, Ser-47, Ser-131, and Ser-172 (score, >0.8). Similarly the phosphorylation server Scansite (55) identified potential phosphorylation sites located at residues Thr-36, Ser-37, and Ser-172 (score, >0.5). From the determined NHE1-CHP1 structure, residues Thr-36, Ser-37, and Ser-172, predicted by both servers as potential phosphorylation sites, are locate at the terminal part of the EF-hand helix or its flanking loop where the side chains of

the aforementioned residues are exposed to the protein surface reinforcing the possibility of phosphorylation. Phosphorylation-induced conformational changes in CHP1 and the subsequent regulation of NHE1 activity are interesting areas that remain to be investigated.

Conclusion—We have determined the solution structure of the cytoplasmic region of NHE1 complexed with CHP1. Although previous biochemical analyses suggested that the hydrophobic residues of NHE1 were likely to interact with CHP1, the present study has delineated the structural basis for this interaction. The solution structure provides concrete evidence that the cytoplasmic region of NHE1 forms an amphipathic helix that interacts directly with the large concave undersurface of CHP1. This helix is disrupted in the absence of CHP1; thus the loss in activity following CHP1 depletion might be due to disruption of the structure of the juxtamembrane region of NHE1. Our structure provides a first step toward understanding the regulation of NHE1 activity. Moreover it revealed a novel target binding mechanism mediated by four EF-hands. These findings should facilitate future studies aimed at understanding the mechanism underlying recognition utilized by EF-hand proteins that are engaged in signal transduction pathways and many other molecular and cellular events. During the initial review of our manuscript, a study appeared that describes a crystal structure of the NHE1 peptide complexed with CHP2 containing Y^{3+} ions instead of Ca^{2+} (56).

Acknowledgments—We are grateful to Momoko Yoneyama, Hiroko Kinoshita, and Junko Tsukamoto of the Nara Institute of Science and Technology for technical assistance and Kokoro Hayashi for help in sample preparation.

REFERENCES

1. Orlowski, J., and Grinstein, S. (2004) *Pfluegers Arch. Eur. J. Physiol.* 447, 549–565
2. Lin, X., and Barber, D. L. (1996) *Proc. Natl. Acad. Sci. U. S. A.* 93, 12631–12636
3. Pang, T., Su, X., Wakabayashi, S., and Shigekawa, M. (2001) *J. Biol. Chem.* 276, 17367–17372
4. Bertrand, B., Wakabayashi, S., Ikeda, T., Pouyssegur, J., and Shigekawa, M. (1994) *J. Biol. Chem.* 269, 13703–13709
5. Wakabayashi, S., Bertrand, B., Ikeda, T., Pouyssegur, J., and Shigekawa M. (1994) *J. Biol. Chem.* 269, 13710–13715
6. Dhanasekaran, N., Prasad, M. V., Wadsworth, S. J., Dermott, J. M., and van Rossum, G. (1994) *J. Biol. Chem.* 269, 11802–11806
7. Hooley, R., Yu, C. Y., Symons, M., and Barber, D. L. (1996) *J. Biol. Chem.* 271, 6152–6158
8. Voyno-Yasenetskaya, T., Conklin, B. R., Gilbert, R. L., Hooley, R., Bourne, H. R., and Barber, D. L. (1994) *J. Biol. Chem.* 269, 4721–4724
9. Bianchini, L., L'Allemain, G., and Pouyssegur, J. (1997) *J. Biol. Chem.* 272, 271–279
10. Takahashi, E., Abe, J., Gallis, B., Aebersold, R., Spring, D. J., Krebs, E. G., and Berk, B. C. (1999) *J. Biol. Chem.* 274, 20206–20214
11. Lehoux, S., Abe, J.-i., Florian, J. A., and Berk, B. C. (2001) *J. Biol. Chem.* 276, 15794–15800
12. Yan, W., Nehrke, K., Choi, J., and Barber, D. L. (2001) *J. Biol. Chem.* 276, 31349–31356
13. Aharonovitz, O., Zaun, H. C., Balla, T., York, J. D., Orlowski, J., and Grinstein, S. (2000) *J. Cell Biol.* 150, 213–224
14. Pang, T., Hisamitsu, T., Mori, H., Shigekawa, M., and Wakabayashi, S. (2004) *Biochemistry* 43, 3628–3636
15. Barroso, M. R., Bernd, K. K., DeWitt, N. D., Chang, A., Mills, K., and Sztul, E. S. (1996) *J. Biol. Chem.* 271, 10183–10187
16. Lin, X., Sikkink, R. A., Rusnak, F., and Barber, D. L. (1999) *J. Biol. Chem.* 274, 36125–36131
17. Timm, S., Titus, B., Bernd, K., and Barroso, M. (1999) *Mol. Biol. Cell* 10, 3473–3488
18. Matsumoto, M., Miyake, Y., Nagita, M., Inoue, H., Shitakubo, D., Takemoto, K., Ohtsuka, C., Murakami, H., Nakamura, N., and Kanazawa, H. (2001) *J. Biochem. (Tokyo)* 130, 217–225
19. Nakamura, N., Miyake, Y., Matsushita, M., Tanaka, S., Inoue, H., and Kanazawa, H. (2002) *J. Biochem. (Tokyo)* 132, 483–491
20. Pang, T., Wakabayashi, S., and Shigekawa, M. (2002) *J. Biol. Chem.* 277, 43771–43777
21. Mailander, J., Muller-Esterl, W., and Dedio, J. (2001) *FEBS Lett.* 507, 331–335
22. Perera, E. M., Martin, H., Seeherunvong, T., Kos, L., Hughes, I. A., Hawkins, J. R., and Berkovitz, G. D. (2001) *Endocrinology* 142, 455–463
23. Naoe, Y., Arita, K., Hashimoto, H., Kanazawa, H., Sato, M., and Shimizu, T. (2005) *J. Biol. Chem.* 280, 32372–32378
24. Yamazaki, T., Lee, W., Arrowsmith, C. H., Muhandiram, D. R., and Kay, L. E. (1994) *J. Am. Chem. Soc.* 116, 11655–11666
25. Matsuo, H., Kupce, E., Li, H., and Wagner, G. (1996) *J. Magn. Reson. B* 111, 194–198
26. Muhandiram, D. R., and Kay, L. E. (1994) *J. Magn. Reson. B* 103, 203–216
27. Clowes, R. T., Boucher, W., Hardman, C. H., Domaille, P. J., and Laue, E. D. (1993) *J. Biomol. NMR* 3, 349–354
28. Kay, L. E., Xu, G. Y., Singer, A. U., Muhandiram, D. R., and Formankay, J. D. (1993) *J. Magn. Reson. B* 101, 333–337
29. Logan, T. M., Olejniczak, E. T., Xu, R. X., and Fesik, S. W. (1993) *J. Biomol. NMR* 3, 225–231
30. Neri, D., Szyperski, T., Otting, G., Senn, H., and Wuthrich, K. (1989) *Biochemistry* 28, 7510–7516
31. Boucher, W., Laue, E. D., Campbell-Burk, S., and Domaille, P. J. (1992) *J. Am. Chem. Soc.* 114, 2262–2264
32. Cavanagh, J., Fairbrother, W. J., Palmer, A. G., III, and Skelton, N. J. (1996) *Protein NMR Spectroscopy*, pp. 301–531, Academic Press, San Diego, CA
33. Grzesiek, S., and Bax, A. (1993) *J. Biomol. NMR* 3, 185–204
34. Delaglio, F., Grzesiek, S., Vuister, G. W., Zhu, G., Pfeifer, J., and Bax, A. (1995) *J. Biomol. NMR* 6, 277–279
35. Goddard, T. D., and Kneller, D. G. (1999) *SPARKY3*, University of California, San Francisco
36. Herrmann, T., Guntert, P., and Wuthrich, K. (2002) *J. Mol. Biol.* 319, 209–227
37. Schwieters, C. D., Kuszewski, J. J., Tjandra, N., and Clore, G. M. (2003) *J. Magn. Reson.* 160, 65–73
38. Laskowski, R. A., Rullmannn, J. A., MacArthur, M. W., Kaptein, R., and Thornton, J. M. (1996) *J. Biomol. NMR* 8, 477–486
39. Koradi, R., Billete, M., and Wuthrich, K. (1996) *J. Mol. Graph.* 14, 51–55
40. Nicholls, A., Sharp, K. A., and Honig, B. (1991) *Proteins Struct. Funct. Genet.* 11, 281–296
41. Pettersen, E. F., Goddard, T. D., Huang, C. C., Couch, G. S., Greenblatt, D. M., Meng, E. C., and Ferrin, T. E. (2004) *J. Comput. Chem.* 25, 1605–1612
42. Goda, N., Tenno, T., Takasu, H., Hiroaki, H., and Shirakawa, M. (2004) *Protein Sci.* 13, 652–658
43. Hoeflich, K. P., and Ikura, M. (2002) *Cell* 108, 739–742
44. Bhattacharya, S., Bunick, C. G., and Chazin, W. J. (2004) *Biochim. Biophys. Acta* 1742, 69–79
45. Zhou, W., Qian, Y., Kunjilwar, K., Pfaffinger, P. J., and Choe, S. (2004) *Neuron* 41, 573–586
46. Griffith, J. P., Kim, J. L., Kim, E. E., Sintchak, M. D., Thomson, J. A., Fitzgibbon, M. J., Fleming, M. A., Caron, P. R., Hsiao, K., and Navia, M. A. (1995) *Cell* 82, 507–522
47. Kissinger, C. R., Parge, H. E., Knighton, D. R., Lewis, C. T., Pelletier, L. A., Tempczyk, A., Kalish, V. J., Tucker, K. D., Showalter, R. E., Moomaw, E. W., Gastinel, L. N., Habuka, N., Chen, X., Maldonado, F., Barker, J. E., Bacquet, R., and Villafranca, J. E. (1995) *Nature* 378, 641–644
48. Yap, K. L., Ames, J. B., Swindells, M. B., and Ikura, M. (1999) *Proteins* 37,

499–507
49. Yap, K. L., Ames, J. B., Swindells, M. B., and Ikura, M. (2002) *Methods Mol. Biol.* 173, 317–324
50. Burgoyne, R. D., and Weiss, J. L. (2001) *Biochem. J.* 353, 1–12
51. Salerno, W. J., Seaver, S. M., Armstrong, B. R., and Radhakrishnan, I. (2004) *Nucleic Acids Res.* 32, W566–W568
52. Baumgartner, M., Patel, H., and Barber, D. L. (2004) *Am. J. Physiol.* 287, C844–C850
53. Denker, S. P., Huang, D. C., Orlowski, J., Furthmayr, H., and Barber, D. L. (2000) *Mol. Cell* 6, 1425–1436
54. Blom, N., Gammeltoft, S., and Brunak, S. (1999) *J. Mol. Biol.* 294, 1351–1362
55. Obenauer, J. C., Cantley, L. C., and Yaffe, M. B. (2003) *Nucleic Acids Res.* 31, 3635–3641
56. Ammar, Y. B., Takeda, S., Hisamitsu, T., Mori, H., and Wakabayashi, S. (2006) *EMBO J.* 25, 2315–2325

Cardiac Ischemia Activates Vascular Endothelial Cadherin Promoter in Both Preexisting Vascular Cells and Bone Marrow Cells Involved in Neovascularization

Naoko Kogata, Yuji Arai, James T. Pearson, Kazuaki Hashimoto, Kyoko Hidaka, Tatsuya Koyama, Satoshi Somekawa, Yoshikazu Nakaoka, Minetaro Ogawa, Ralf H. Adams, Masato Okada, Naoki Mochizuki

Abstract—Vascular endothelial cadherin (VE-cadherin) is expressed on vascular endothelial cells, which are involved in developmental vessel formation. However, it remains elusive how VE-cadherin–expressing cells function in postnatal neovascularization. To trace VE-cadherin–expressing cells, we developed mice expressing either green fluorescent protein or LacZ driven by VE-cadherin promoter using Cre-loxP system. Although VE-cadherin promoter is less active after birth than during embryogenesis in blood vessels, it is reactivated on cardiac ischemia. Both types of reporter-positive cells are found in the vasculature and in the infarcted myocardium. Those found in the vasculature were pre-existing endothelial cells and incorporated endothelial progenitor cells derived from extracardiac tissue. In addition to the vasculature, VE-cadherin promoter-activated cells were positive for CD45 in the bone marrow cells of the infarcted mice. VE-cadherin promoter–reactivated CD45-positive leukocytes were also found in the infarcted area. In addition, VE-cadherin promoter was activated in the bone marrow vessels of the infarcted mice. Collectively, our findings reveal a new ischemia-induced neovascularization mechanism involving VE-cadherin: the re-expressed VE-cadherin–mediated cell adhesion between cells may be involved not only in homing of bone marrow–derived cells to ischemic area but also mobilization from bone marrow. (*Circ Res.* **2006;98:897-904.**)

Key Words: vasculogenesis ■ angiogenesis ■ hemangioblast ■ ischemia ■ CD45

Cell-based therapies have been aimed at neovascularization in ischemic diseases.[1] Recruitment of both angiogenic factor-producing hematopoietic cells and vasculature-constituting endothelial cells to the ischemic area contributes to neovascularization.[2] Endothelial progenitor cells (EPCs) and circulating bone marrow–derived EPCs (CEPCs) are incorporated into the nascent vessels.[3,4] These cells have been suggested to originate from bone marrow. On the basis of this potential differentiation capability, bone marrow cell–based therapy has been attempted and proven to be effective for ischemic heart disease and peripheral artery disease.[5,6] However, it is unclear how bone marrow–derived cells are recruited to the ischemic area.

Postnatal neovascularization includes angiogenesis and vasculogenesis. Both steps cooperatively work by involving the sprouting and branching of the pre-existing endothelial cells and recruiting EPCs in the vascular tree.[7] Proangiogenic factors released from ischemic tissue and infiltrating cells, including vascular endothelial growth factor (VEGF), fibroblast growth factor, granulocyte macrophage colony-stimulating factor, and placental growth factor, mobilize hematopoietic stem cells (HPCs) as well as EPCs to the infarcted area.[8–10] Thus, HPCs and EPCs homing to the ischemic area are involved in angiogenesis and vasculogenesis in coordination with pre-existing vascular cells. Similar to adult neovascularization, embryonic vasculogenesis and angiogenesis are coordinated by both endothelial lineage cells and hematopoietic cells originating from hemangioblasts.

Several cell surface molecules, including CD133, VEGF receptor 2, vascular endothelial cadherin (VE-cadherin), and CD34, have been used to characterize the EPCs in the bone marrow and CEPCs in the peripheral blood.[6] Although the cells purified by cell surface marker have been demonstrated to be recruited to the ischemic area when transferred for cell-based therapy, it is elusive how and what endogenous EPCs, CEPCs, and HPCs are mobilized to ischemic area for neovascularization in ischemic diseases.

VE-cadherin (Cadherin5, CD144), which belongs to cadherin super family, is expressed on cultured vascular endothelial cells and is essential for endothelial cell–cell interaction.[11] Whereas N-cadherin, another cadherin expressed on the endothelial cells, is thought to function in adherens

Original received April 20, 2005; revision received February 28, 2006; accepted March 8, 2006.

From the Departments of Structural Analysis (N.K., Y.N., T.K., S.S., N.M.), Bioscience (Y.A., K.H.), and Cardiac Physiology (J.T.P.); National Cardiovascular Center Research Institute, Osaka, Japan; the Department of Cell Differentiation, Institute for Molecular Embryology and Genetics (K.H., M.O.), Kumamoto University, Kumamoto, Japan; the Vascular Development Laboratory (R.H.A.), Cancer Research UK London Research Institute, United Kingdom; and the Department of Oncogene Research (M.O.), Institute for Microbial Disease, Osaka University, Japan.

Correspondence to Naoki Mochizuki, Department of Structural Analysis, National Cardiovascular Center Research Institute, 5-7-1 Fujishirodai, Suita, Osaka 565-8565, Japan. E-mail nmochizu@ri.ncvc.go.jp

Circulation Research is available at http://circres.ahajournals.org DOI: 10.1161/01.RES.0000218193.51136.ad

junctions between endothelial cells and mural cells (pericytes and vascular smooth muscle cells [VSMCs]).[12] VE-cadherin is required in vivo in the postnatal vasculature to maintain endothelial cell integrity and barrier function.[13,14] Moreover, VE-cadherin associated with VEGF receptor is involved in the regulation of permeability after myocardial ischemia.[15]

In the present study, we investigated the role of VE-cadherin promoter-activated cells in ischemia-induced neovascularization. We demonstrate that VE-cadherin promoter is activated in the pre-existing vascular endothelial cells of bone marrow and heart. In addition, we noticed VE-cadherin promoter is activated in the bone marrow cells and peripheral blood cells presumably corresponding to EPCs/CEPCs and CD45-positive cells preferentially homing to infarcted heart. Thus, we raise the possibility of VE-cadherin–mediated cell–cell contact for effective homing of proangiogenic cells to ischemic tissues.

Materials and Methods

Generation of Transgenic Mice

Cre recombinase driven by VE-cadherin promoter (VE-cad-Cre) mice contained the 4.2-kb VE-cad-Cre transgene (Figure 1A) excised from pBluescript-VE-cad-Cre (online supplement, available at http://circres.ahajournals.org). VE-cad-Cre mice were crossed with LacZ reporter mice (cAct-XstopX-LacZ from the Jackson Laboratory, Bar Harbor, Me) or enhanced green fluorescent protein (GFP) reporter mice (CAG-CAT–enhanced GFP [EGFP] obtained from J. Miyazaki, Osaka University).[16] The offspring were named VE-cadherin promoter-driven LacZ-expressing mice (VE/Z) and VE-cadherin promoter-driven EGFP-expressing mice (VE/EG), respectively. All animal experiments were approved by the animal committee of the National Cardiovascular Center and performed according to the regulation of the National Cardiovascular Center.

Detection of Fluorescence In Vivo

VE/EG embryos and dissected organs from VE/EG mice were examined using an Olympus SZX12 stereo-fluorescent microscope equipped with a VB-6010 charge-coupled device camera. The organs from control mice were imaged next to those from VE/EG mice.

Histochemistry, Immunostaining, Immunofluorescence, and In Situ Hybridization

The procedures of histological examination are described in the online supplement.

Neovascularization Models

To monitor VE-cadherin promoter–activated cells during neovascularization, we used a corneal angiogenesis model of 8-week-old VE/EG mouse and myocardial infarction model. Both methods are described in the online supplement.

Parabiosis Model

Pairs of a 6- to 10-week-old wild-type and VE/Z mice were subjected to parabiotic surgery. Mice were surgically joined from shoulder to femur. One week after parabiotic surgery, the coronary artery was ligated in the wild-type mouse.

Characterization of EGFP-Expressing Cells by Flow Cytometric Analysis

EGFP expression of these cells was analyzed by FACS (fluorescence-activated cell sorting) Calibur (BD Biosciences). EGFP together with cell surface antigen immunostained with phycoerythrin-conjugated anti-CD31 or anti-CD45 were investigated using FACS VantageSE or FACS Aria (BD Biosciences).

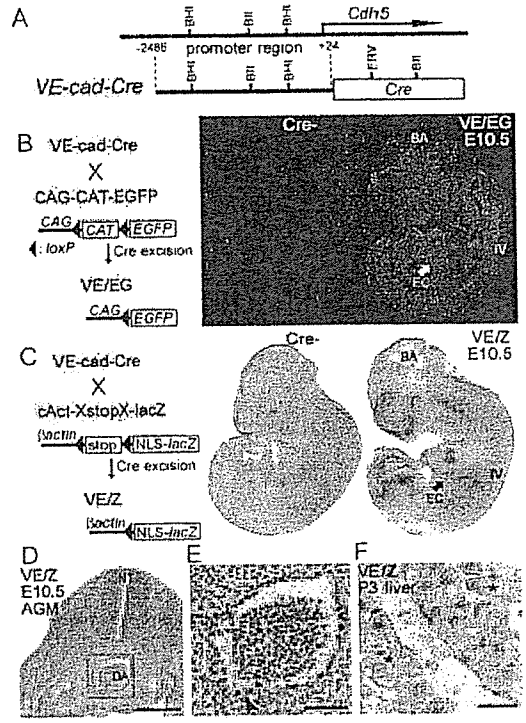

Figure 1. VE-cadherin (Cadherin5, Cdh5) promoter is activated during developmental vascularization. A, VE-cadherin promoter-driven Cre recombinase expressing mouse. BHI, Bam HI; BII, BglII; ERV, EcoRV. B, VE-cadherin promoter-dependent EGFP-expressing mouse (VE/EG). EGFP was expressed in intersomitic vessels (IV), and basilar artery (BA), and endocardium (EC) of VE/EG mice at embryonic day 10.5 (E10.5). No EGFP expression in a littermate lacking *Cre* gene (Cre-). C, VE-cadherin–dependent LacZ-expressing mouse (VE/Z). Whole-mount X-gal staining of E10.5 VE/Z mice shows similar reporter expression to VE/EG. NLS indicates nuclear localization signal. D, Cross-section of neural tube, dorsal aorta, and somites of E10.5 VE/Z embryo shows LacZ-positive signals in dorsal aorta (DA). Bar=200 μm. E, Box in D is enlarged. LacZ-positive cells are present in the hematopoietic cells in the dorsal aorta lumen and its lining cells (arrowhead). Bar=50 μm. F, In the liver, LacZ-expressing cells are detected in the sinusoidal endothelium and the scattered cells, which seem to be hematopoietic cells (asterisks). Bar=20 μm.

Results

VE-Cadherin Promoter Is Activated in Cells Responsible for Developmental Vessel Formation

To trace the VE-cadherin–expressing cells in fetal vascular development and postnatal neovascularization, we first generated transgenic mice expressing VE-cad-Cre (Figure 1A). By crossing three lines of VE-cad-Cre mice with either EGFP reporter mice or LacZ reporter mice, we obtained VE/EG and VE/Z (Figure 1B and 1C).

EGFP and LacZ expression by VE-cad-Cre–mediated recombination was observed in embryonic vascular development (Figure 1B and 1C). We examined LacZ expression in Aorta-Gonad-Mesonephros (AGM) region of VE/Z mice where hemangioblasts reside.[17,18] LacZ-positive cells were detected in the dorsal aorta (Figure 1D, boxed). We noticed that LacZ-stained cells were in the lumen and in the lining cells of the ventral wall (Figure 1E, arrowhead) and in the cells that seemed to bud off from the inner layer. LacZ-

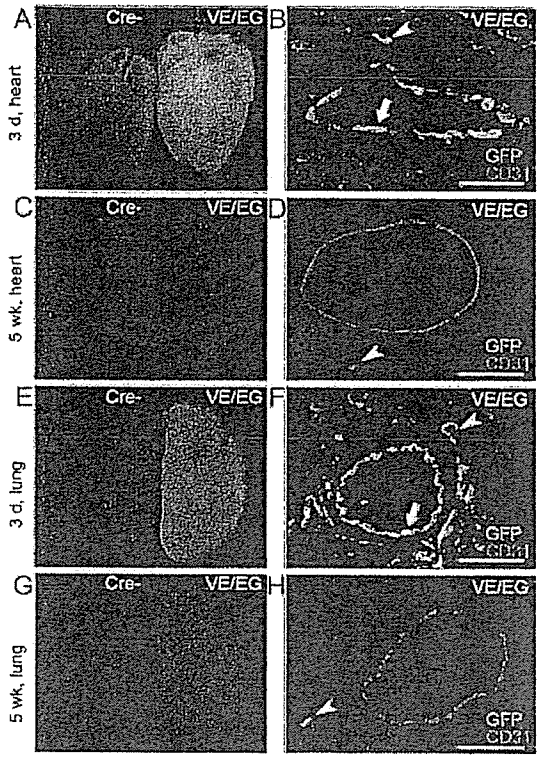

Figure 2. VE-cadherin promoter is less activated after birth than before birth. Organs from littermates lacking *Cre* gene (Cre-) do not show any EGFP expression (A, C, E, and G). A, EGFP is observed in the heart of newborn (3 days after birth) VE/EG mice. B, In the section of a newborn VE/EG mouse heart, EGFP is detected by anti-GFP (green) among the CD31-positive (red) arterial vascular endothelial cells (arrow) and capillary endothelial cells (arrowhead). Positive immunoreaction for anti-GFP and anti-CD31 is visualized by Alexa488-conjugated goat anti-rabbit antibody (green) and Alexa 546-conjugated anti-mouse antibody (red), respectively. C, EGFP is not expressed in the 5-week-old VE/EG mouse heart. D, A few EGFP-positive cells (arrowhead) are detected in capillaries of 5-week-old VE/EG mice. E, Similar to the heart, EGFP is observed in the newborn VE/EG mouse lung. F, EGFP (green) is merged with CD31-positive (red) arterial endothelial cells (arrow) and capillary endothelial cells (arrowhead). G, Lungs of 5-week-old VE/EG mice do not express EGFP. H, A few EGFP-positive cells (arrowhead) were detected in capillaries of the VE/EG mouse lung. Bar=50 μm.

stained cells were also found in the newborn VE/Z mouse liver, where hepatic hematopoiesis is organized (Figure 1F, asterisks). These results suggest that VE-cadherin promoter is activated in the cells probably corresponding to hemangioblasts responsible for fetal vasculogenesis.

VE-Cadherin Promoter Becomes Less Active After Birth

To assess the involvement of VE-cadherin in postnatal vascular development, we examined changes in EGFP reporter expression with age in tissues. Although EGFP expression in both neonatal heart and lung was noticeable, its expression was gradually decreased by aging and no longer observed by the fifth week (Figure 2A, 2C, 2E, and 2G). EGFP and CD31 (platelet and endothelial cell adhesion molecule-1) expression overlapped in the vascular endothelium of both heart and lung of the neonatal VE/EG mice, as revealed by immunohistochemical analyses using anti-GFP

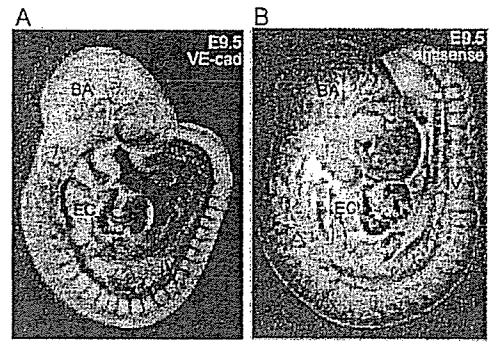

Figure 3. VE-cadherin expression and VE-cadherin mRNA expression in embryogenesis. A, VE-cadherin is detected in the basilar arteries (BA), endocardium (EC), and intersomitic vessels (IV) by immunohistochemistry in an embryonic 9.5 (E9.5) wild-type mouse embryo using anti–VE-cadherin antibody. B, In situ hybridization using antisense probe for VE-cadherin mRNA reveals that VE-cadherin mRNA is expressed in BA, EC, and IV of an E9.5 wild-type mouse embryo. Sense probe used as a negative control does not detect any VE-cadherin mRNA (data not shown). Bar=50 μm.

and anti-CD31 antibodies (Figure 2B and 2F). In clear contrast, GFP was not detected in the CD31-positive vascular endothelium of 5-week-old VE/EG mice (Figure 2D and 2H). Similarly, we found that EGFP expression was decreased with age in other organs, including the brain, liver, and kidney (data not shown).

Tie2 is a tyrosine kinase receptor for angiopoietin and is expressed in the endothelial cells and hematopoietic cells.[19] Thus, we further compared the VE-cadherin promoter-dependent EGFP expression with that dependent on Tie2 promoter. EGFP expression persisted through the entire life (supplemental Figure II), supporting that the VE-cadherin promoter is more active during embryonic and prenatal vascularization than postnatal vessel maintenance. Similarly, VE-cadherin promoter-driven LacZ expression was decreased with aging (supplemental Figure II).

VE-Cadherin Is Expressed in Developing Vasculature

To confirm that VE-cadherin promoter-driven EGFP and LacZ reporter expression reflects endogenous VE-cadherin expression in vivo, we examined the expression of VE-cadherin and VE-cadherin mRNA in embryo. VE-cadherin, VE-cadherin mRNA was detected in developing vessels of the embryo stained with anti–VE-cadherin antibody (Figure 3A) and of the embryo probed with antisense–VE-cadherin cDNA (Figure 3B). VE-cadherin protein and VE-cadherin mRNA were detected in the basilar arteries, intersomitic vessels, and endocardium as reporters of VE/EG and VE/Z mice were expressed. These results indicate that VE-cadherin promoter-driven reporter expression of both VE/EG and VE/Z mice reflects the endogenous VE-cadherin expression.

VE-Cadherin Promoter-Activated Cells Are Involved in Neovascularization

EPCs are positive for VE-cadherin and involved in neovascularization.[6] We hypothesized that VE-cadherin promoter is turned on in EPCs during adult vasculogenesis and that VE-cadherin promoter may be reactivated in vessels. There-

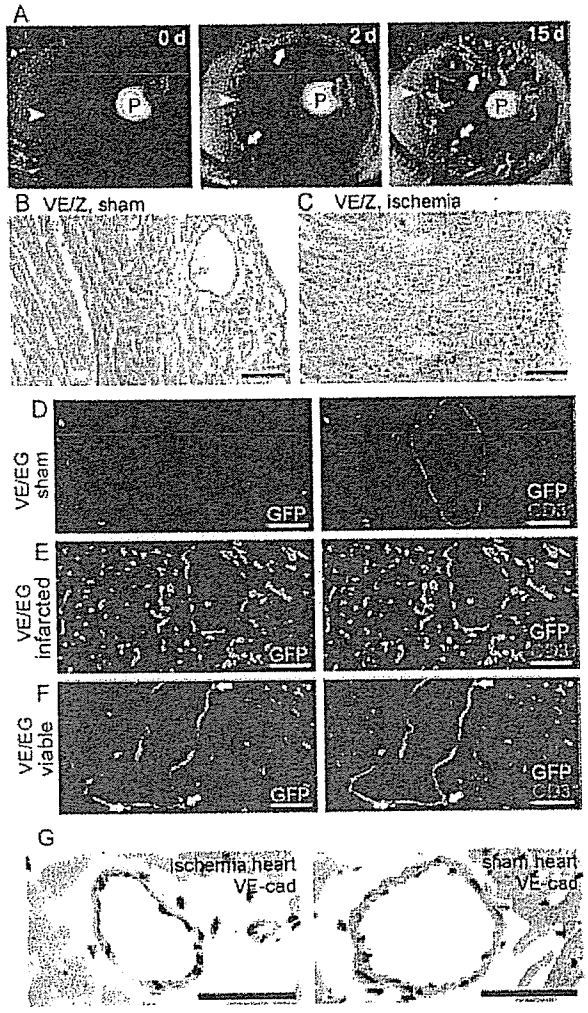

Figure 4. Reactivation of VE-cadherin promoter in response to VEGF and cardiac ischemia. A, New vessel formation monitored by EGFP expression in the VE/EG mouse cornea just 0 days (0 d), 2 days (2 d), and 15 days (15 d) after the implantation of a VEGF-containing pellet (P). Arrowheads and arrows denote the limbus vessels and nascent vessels, respectively. B, Section of sham coronary-ligated VE/Z mouse shows no LacZ-stained cells in the heart. Bar=100 μm C, Numerous LacZ-stained cells are present in the infarcted region of the VE/Z mouse 3 days after coronary ligation. Bar=100 μm. D, The section of the sham-operated VE/EG mouse heart was immunostained with anti-GFP and anti-CD31. Similar to Figure 2, Alexa488 image and that merged with Alexa546 image are shown in the left and right panels, respectively. E, Immunostaining similar to D shows partial colocalization of GFP (green) and CD31 (red) in the infarcted area of VE/EG mouse heart. F, Colocalization of GFP (green) and CD31 (red) in the both arteries and capillaries in the viable area surrounding the infarcted area. Arrowheads denote the GFP-positive cells outside of the endothelium and inside of vascular wall. Bars (in D, E, and F)=50 μm. G, VE-cadherin is detected (brown) in the vessels of infarcted heart but not sham-operated heart. Bar=25 μm.

fore, we first tested whether VEGF induces EGFP expression in using a cornea model of VE/EG mice. After implanting VEGF-containing pellets, EGFP expression was monitored every day. Not only new vessels growing toward the implanted pellets but also limbus vessels exhibited EGFP expression (Figure 4A), indicating that VE-cadherin promoter is activated in the vascular cells involved in neovascularization.

We next tested whether ischemia triggers VE-cadherin expression in a myocardial infarction model. When the coronary artery of VE/Z mice was ligated, LacZ-positive cells were found 3 days after coronary ligation in the hearts of the infarcted mice but not those in the sham-operated mice (Figure 4B and 4C). Similarly, EGFP expression was examined by immunohistochemistry using anti-GFP antibody. In sham-operated control VE/EG mice, GFP-positive cells were not detected in the heart except a few capillaries (Figure 4D), whereas GFP-positive cells were observed in the infarcted area (Figure 4E, left). Notably, among GFP-positive cells, we found CD31-positive cells in the merged image (Figure 4E, right). More than 50% of GFP-positive cells were negative for CD31, suggesting that GFP-positive cells may include nonendothelial lineage cells. Intriguingly, the endothelial cells lining the vessels marked by CD31 in the adjacent viable region were positive for GFP (Figure 4F). In addition, we could find GFP-positive cells in the nonendothelial cell layer in the arterial walls, probably smooth muscle cell layer in the viable area (Figure 4F, arrows). Consistent with GFP reporter expression, VE-cadherin was detected by immunohistochemistry in the endothelium and smooth muscle cells in the vessels of the infarcted heart but not in the sham-operated heart (Figure 4G).

Ischemia Triggers VE-Cadherin Expression in Preexisting Vascular Cells and Mobilized Cells

To test whether the VE-cadherin promoter-activated cells are derived from extracardiac tissues of infarcted mice, we used a parabiotic pairing between a wild-type mouse and a VE/Z mouse (Figure 5, gray mouse and blue mouse, respectively). In a parabiotic mice model, circulating blood cells are mixed through vascular anastomoses that form between the two mice.[20,21] LacZ-positive cells were found in both endothelial cell layer and smooth muscle cell layer of infarcted VE/Z mouse (Figure 5A, arrowhead and arrow, respectively), as confirmed by the same section immunostained with anti-CD31 and anti-α-smooth muscle actin (SMA). In a parabiosis model in which the wild-type mouse was coronary ligated (indicated by cross), we observed that LacZ-positive cells were recruited to the infarcted area of the wild-type mouse (Figure 5B, denoted by cross) from the VE/Z mice (Figure 5B, left). These results indicate that VE-cadherin promoter-reactivated cells are derived from extracardiac tissues and subsequently home to the infarcted heart. Notably, these LacZ-stained cells were negative for CD31 or α-SMA (Figure 5B, right). These results were consistent with those found in the infarcted area of VE/EG mice (Figure 4E). In addition to the infarcted area, LacZ-positive cells were incorporated in the vascular endothelial cell layer and VSMC layer of the viable area (Figure 5C and D), although the number of LacZ-positive cells were much less than that of unconnected mouse. Given that most of the endothelial cells lining the vessels of viable area of infarcted VE/EG mice were positive for GFP (Figure 4E) and that the number of LacZ-positive cells found in the vessels were much less in parabiotic model, VE-cadherin promoter is activated in the pre-existing vessels

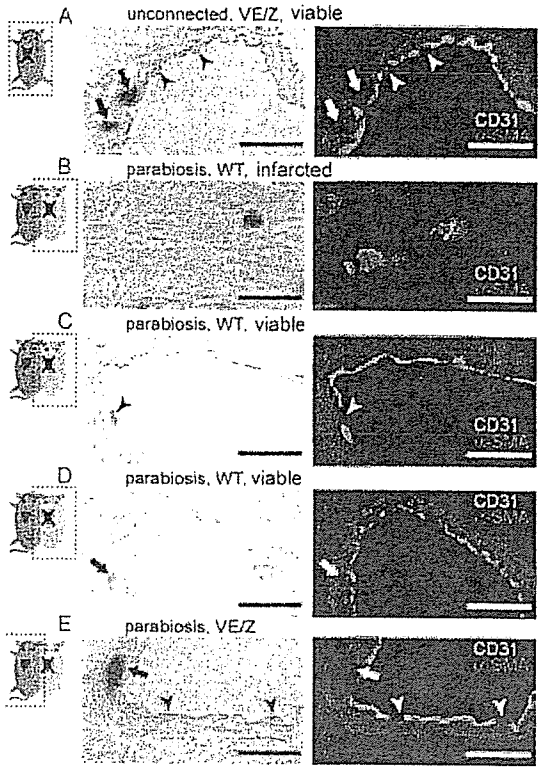

Figure 5. Ischemia induces the recruitment of circulating VE-cadherin promoter-activated cells. Sections show tissues for the mouse indicated by the broken line box. In all panels, crosses indicate coronary ligation, and arrowheads and arrows denote LacZ/CD31-positive and LacZ/α-SMA–positive cells, respectively. All images were obtained by a confocal microscope (LSM510 META; Carl Zeiss). A, LacZ-stained cells in both α-SMA–positive cell layer and CD31-positive cell layer in the arteries of the viable area of infarcted VE/Z mice (cross). B, C, D, and E, A parabiotic pairing between a wild-type (WT) mouse (gray) and a VE/Z mouse (blue). B, Sections of the infarcted heart region of the wild-type mouse were examined for LacZ expression. LacZ-positive cells are negative for CD31 and α-SMA. C and D, In the same model as B, LacZ expression was examined in variable area of infarcted wild-type mouse. E, Coronary arteries of the noninfarcted VE/Z mouse were examined for LacZ expression. Bars=10 μm.

of viable area. Collectively, these data indicate that VE-cadherin–expressing cells, which do not correspond to vascular cells, are recruited to infarcted area from extracardiac tissue. Notably, when examining the heart of the donor VE/Z mouse without myocardial infarction, LacZ-stained cells were found in both endothelial cell layer and VSMC layer in spite of the absence of cardiac ischemia (Figure 5E), indicating that circulating stimuli may activate VE-cadherin promoter in either the pre-existing vascular cells or the mobilized cells from extracardiac tissue to the vasculature. Parabiosis itself did not trigger LacZ expression before the ischemia (supplemental Figure IIIA). Cardiac ischemia, not but other organ ischemia, is critical for VE-cadherin expression in the heart (supplemental Figure III).

VE-Cadherin Promoter Is Activated in Bone Marrow Cells and Circulating Blood Cells on Myocardial Ischemia

To investigate the origin of the cells homing to the ischemic tissues from extracardiac tissue, we explored EGFP-expressing cells in bone marrow and peripheral blood of the infarcted VE/EG mice by flow cytometry. Although EGFP-expressing cells were not detected in the bone marrow of the sham-operated mice, EGFP-expressing bone marrow cells increased after coronary ligation and reached 5% of total bone marrow mononuclear cells (Figure 6A and 6B). In parallel with the increase of EGFP-expressing cells in bone marrow, EGFP-expressing cells also increased in the peripheral blood (Figure 6C). No EGFP-expressing cells were detected in the blood from sham-operated mice. EGFP-expressing cells increased up to 6% of total circulating mononuclear cells 7 days after ligation (Figure 6D).

EGFP-expressing cells were observed in situ in the vasculature as well as in the marrow cells of infarcted VE/EG mice (Figure 6F) but not in sham-operated mice (Figure 6E), suggesting that VE-cadherin–mediated cell adhesion may be involved in mobilization of bone marrow cells into the bloodstream.

We further examined the expression of endogenous VE-cadherin in the EGFP-expressing cells sorted from the bone marrow of infarcted VE/EG mice. More than 90% and 40% of EGFP-expressing cells were positive for VE-cadherin and for CD31, respectively (Figure 6G and 6H). These data indicate that EGFP reporter expression reflects endogenous VE-cadherin expression in bone marrow cells. To characterize the CD31-negative cells, we performed flow cytometric analysis on mononuclear bone marrow cells obtained from infarcted VE/EG mice 2 days after coronary ligation using anti-CD31 and anti-CD45 because CD45 is expressed in the common origin of both myeloid cells and endothelial cells.[5] Among EGFP-positive cells, 50% were positive for CD31, in agreement with the immunostaining of GFP-positive cells with anti-CD31 (Figure 6H and 6I). Of note, all EGFP-expressing cells were positive for the pan-leukocyte cell marker CD45. VE-cadherin mRNAs of bone marrow CD45-positive cells of infarcted mice were twice as much as those of sham-operated mice (supplemental Figure V). These results indicate that EGFP-expressing cells consist of either multilineage cells or distinct stages of differentiated cell from a common origin: CD45-positive EPCs, CD45-positive hematopoietic precursor cells, and CD45-positive hematopoietic cells.

VE-Cadherin Promoter-Activated CD45-Positive Cells Are Actively Recruited to Ischemic Area

We found that VE-cadherin promoter-activated cells were positive for CD45 (Figure 6I) and that CD31-negative GFP-expressing cells were detected in the infarcted area (Figure 4E). Thus, we assumed that CD31-negative GFP-expressing cells might be CD45-positive cells in the infarcted heart. The heart of the infarcted VE/EG mice were immunostained with anti-GFP and anti-CD45. Double-positive staining was found in cells other than elongated cells that seemed to be endothelial cells (Figure 7A). The percentage of double-positive cells among CD45-positive cells in the infarcted area (>10% of CD45-positive cells were positive for GFP) was greater than that of CD45/EGFP-expressing cells in bone marrow cells as examined by FACS analysis (≈1.5% of CD45-positive cells were GFP positive; Figure 6I), indicating that double-positive

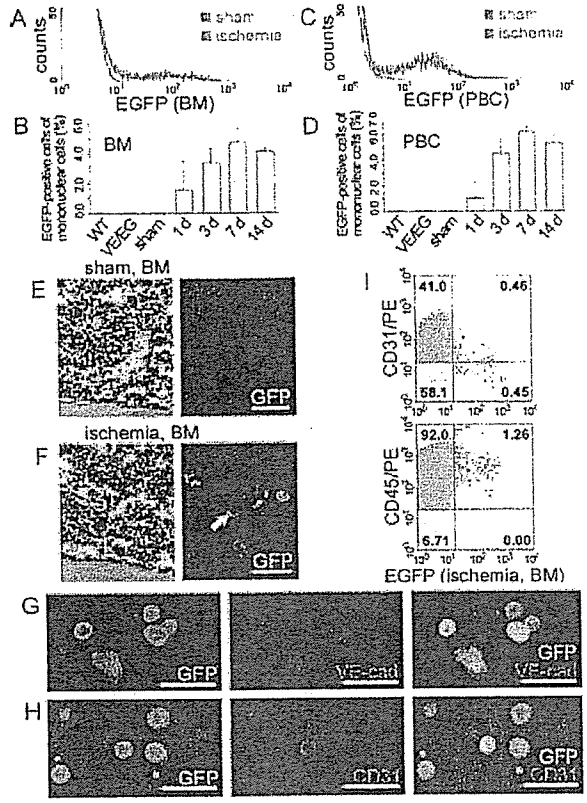

Figure 6. Ischemia induces increases in VE-cadherin promoter-activated bone marrow cells and blood cells. A, Flow cytometric analysis reveals EGFP-expressing cells appearing in bone marrow (BM) 3 days after coronary artery ligation in a VE/EG mouse (green) but not in a sham-operated VE/EG mouse (gray). B, EGFP-expressing cells in bone marrow cells obtained from the infarcted VE/EG mice were counted by flow cytometry. WT indicates wild-type mice; VE/EG, VE/EG mice without any operation; sham, sham-operated VE/EG mice; 1 d, 3 d, 7 d, and 14 d: 1 day, 3 days, 7 days, and 14 days after coronary ligation of VE/EG mice, respectively (n=3). C, Similar to A, EGFP-expressing cells increased in peripheral blood cells (PBC) of the coronary-ligated VE/EG mouse (green) but not in the sham-operated mouse (gray). D, Similar to B, EGFP-expressing peripheral blood cells obtained from infarcted mice were analyzed by flow cytometry. E, Expression of VE-cadherin in BM of sham-operated VE/EG mouse examined by immunostaining with anti-GFP. F, Similar to E, VE-cadherin promoter-reactivated cells were examined in the infarcted VE/EG mouse BM. Arrowheads indicate the immunopositive signal (green) in the endothelium of vessels. Bar=50 μm. G, EGFP-expressing cells obtained by cell sorting from the BM of VE/EG mouse 3 days after coronary ligation were immunostained with anti-GFP (left) and anti–VE-cadherin (center). The GFP image (green) and VE-cadherin image (red) is merged (right). A representative result of more than three independent experiments is shown. H, EGFP-expressing cells obtained from the same mouse as in G were immunostained with anti-GFP (left) and anti-CD31 (center). The merged image is shown in the right panel. I, Bone marrow cells obtained from an infarcted VE/EG mouse 2 days after coronary ligation were immunostained with phycoerythrin (PE)-conjugated anti-CD31 (top) or PE-conjugated anti-CD45 (bottom) and subjected to FACS analysis. Numbers indicate the percentage of cells in the fraction. A representative result of more than three independent experiments is shown.

cells were more selectively recruited to the ischemic area than single CD45-positive cells.

Discussion

Here we show for the first time that VE-cadherin promoter-activated cells are detected in both bone marrow cells and

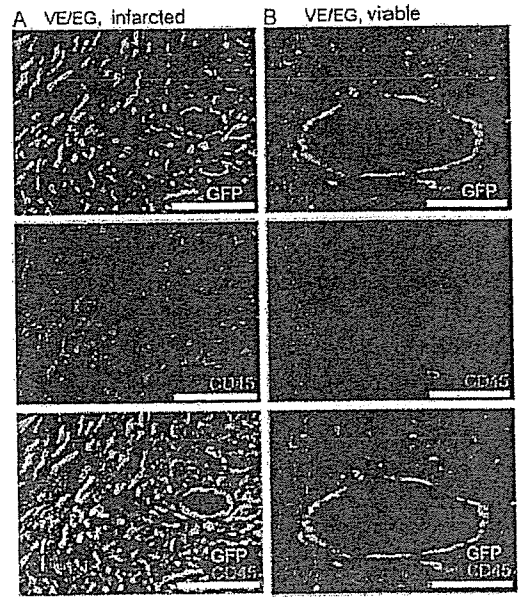

Figure 7. VE-cadherin promoter-activated CD45-positive cells after cardiac ischemia migrate to the infarcted area. A, The infarcted area of the mouse heart immunostained with anti-GFP (top) and anti-CD45 (middle). The GFP image and the CD45 image are merged (bottom). B, The viable area of the same mouse heart was also immunostained with anti-GFP (top), anti-CD45 (middle), and merged (bottom). Bar=100 μm.

blood vessels in the infarcted mice. Although VE-cadherin promoter is less active with aging, reactivated VE-cadherin promoter drives VE-cadherin expression in the pre-existing vessels of ischemic hearts. Our results do not suggest that VE-cadherin is not expressed in mature vessels but rather suggests that VE-cadherin expression is enhanced during ischemia, as detected by anti–VE-cadherin antibody (Figure 4G). Although VE-cadherin is required in the postnatal vascular endothelial cell integrity,[13,14] VE-cadherin is hardly detectable by immunohistochemistry.[22] Ischemia may drive VE-cadherin promoter, resulting in detectable increased VE-cadherin expression in the pre-existing vessels.

What is the role of re-expressed VE-cadherin of the vascular vessels during ischemia? VE-cadherin expression during ischemia may make conditions favorable for the homing of EPCs/CEPCs and the integration of these cells to create the neovessels. VE-cadherin may function not only as an endothelial cell–cell adhesion molecule, but as a leukocyte–endothelial cell adhesion molecule. Leukocytes extravasate across the endothelial cell layer via homophilic platelet and endothelial cell adhesion molecule-1 (CD31), binding between leukocytes and vascular endothelial cells because leukocytes do not express VE-cadherin.[23,24] Because VE-cadherin promoter was activated in CD45-positive leukocytes on ischemia, VE-cadherin on both pre-existing vessels and CD45-positive cells may help to the extravasation of CD45-positive cells.

We noticed that ischemia induced VE-cadherin promoter activation of both marrow cells and endothelium in the bone (Figure 6F). In addition, VE-cadherin promoter-activated marrow cells were positive for VE-cadherin (Figure 6G). VE-cadherin re-expression induced by ischemia appears to pro-

mote the mobilization of VE-cadherin–expressing cells from bone marrow because VE-cadherin regulates the mobilization of bone marrow cells across bone marrow endothelium.[25] Angiopoietin-1/Tie2 signaling maintains an HPC quiescence in bone marrow, probably by regulating N-cadherin.[26] Thus, ischemia may trigger the cadherin switch from N-cadherin to VE-cadherin in cells mobilizing from the bone marrow niche. These CD45-positive cells may function as proangiogenic factor-producing cells at the ischemic tissue.

VE-cadherin may be expressed in both prenatal and postnatal hemangioblasts. In embryos and embryonic stem cells, VE-cadherin–expressing cells have the potential to generate hematopoietic precursors,[27–29] which exist and repopulate in the AGM to differentiate into both hematopoietic cells and endothelial cells.[17] Consistently, we found LacZ-positive cells in the lumen of dorsal aorta and those budding from the lining cells of the dorsal aorta (Figure 1D and 1E). Moreover, no blood cells were found within VE-cadherin–deficient embryos, in addition to impaired vascularization.[30] During embryogenesis, vasculogenesis and hematopoiesis are coordinated by hemangioblasts residing in AGM region, including the dorsal aorta.[31] VE-cadherin–expressing cells may function as adult hemangioblasts because VE-cadherin promoter–activated cells were positive for both CD31 and CD45. It should be tested in the future whether GFP-expressing CD45-positive cells in the infarcted area function as cytokine-secreting cells because EPCs are derived from monocytes and secrete angiogenic factors.[2]

It has been controversial whether bone marrow–derived cells are integrated into vasculature.[32,33] By using parabiotic mice model, we demonstrated that cells from extracardiac tissues were incorporated into both pre-existing endothelial cell and VSMC layers (Figure 5C and 5D). Furthermore, we detected VE-cadherin in both vascular layers of infarcted mice (Figure 4G). VE-cadherin promoter-activated cell detected among smooth muscle cells may be either incorporated cell or pre-existing smooth muscle cells. The former cell may use VE-cadherin–dependent cell–cell interaction for incorporation into the smooth muscle layer across the VE-cadherin–expressing endothelial cells on ischemia. Both endothelial cells and VSMCs originate from the same lineage serving as vascular progenitor cells in embryonic stem cells.[34] Even mature vascular endothelial cells can differentiate into smooth muscle cell.[35] It will be necessary to test whether VE-cadherin promoter-activated cells can give rise to the smooth muscle cells to examine the potential function as vascular progenitor cells.

We obtained the data indicative of unidentified factors that drives VE-cadherin promoter in bone marrow and heart. VEGF-induced mobilization of EPCs depends on the expression of Flk-1 expressed on the EPCs as placental growth factor recruits HPCs that express Flt-1.[8,36] It is of note that we find that circulating factors affect the activity of VE-cadherin promoter just in the vessels of the heart, without affecting activity in other organs (supplemental Figure III). By identifying VE-cadherin promoter-activating factors, we may augment neovascularization in combination with EPC-based cell therapy.

In conclusion, VE-cadherin promoter is reactivated in the ischemic tissue vessels and bone marrow–derived cells. Thus, reactivation of VE-cadherin may be involved in the integration of vessel-constituting cells and angiogenic factor–producing cells.

Acknowledgments

This work was supported by grants from the Ministry of Health, Labor, and Welfare of Japan, from the Program for Promotion of Fundamental Studies in Health Sciences of the National Institute of Biomedical Innovation (NIBIO), from the Ministry of Education, Science, Sports and Culture of Japan, and from Takeda Medical Research Foundation. We thank M. Matsuda for comments; S.I. Nishikawa and D. Vestweber for antibodies; P. Huber for VE-cadherin promoter DNA; M. Yanagisawa, and J. Miyazaki for mice; and M. Miyabayashi, and Y. Matsuura for technical assistance.

References

1. Losordo DW, Dimmeler S. Therapeutic angiogenesis and vasculogenesis for ischemic disease: part II: cell-based therapies. *Circulation*. 2004;109:2692–2697.
2. Rehman J, Li J, Orschell CM, March KL. Peripheral blood "endothelial progenitor cells" are derived from monocyte/macrophages and secrete angiogenic growth factors. *Circulation*. 2003;107:1164–1169.
3. Asahara T, Murohara T, Sullivan A, Silver M, van der Zee R, Li T, Witzenbichler B, Schatteman G, Isner JM. Isolation of putative progenitor endothelial cells for angiogenesis. *Science*. 1997;275:964–967.
4. Shi Q, Rafii S, Wu MH, Wijelath ES, Yu C, Ishida A, Fujita Y, Kothari S, Mohle R, Sauvage LR, Moore MA, Storb RF, Hammond WP. Evidence for circulating bone marrow-derived endothelial cells. *Blood*. 1998;92:362–367.
5. Urbich C, Dimmeler S. Endothelial progenitor cells: characterization and role in vascular biology. *Circ Res*. 2004;95:343–353.
6. Rafii S, Lyden D. Therapeutic stem and progenitor cell transplantation for organ vascularization and regeneration. *Nat Med*. 2003;9:702–712.
7. Carmeliet P. Mechanisms of angiogenesis and arteriogenesis. *Nat Med*. 2000;6:389–395.
8. Hattori K, Heissig B, Wu Y, Dias S, Tejada R, Ferris B, Hicklin DJ, Zhu Z, Bohlen P, Witte L, Hendrikx J, Hackett NR, Crystal RG, Moore MA, Werb Z, Lyden D, Rafii S. Placental growth factor reconstitutes hematopoiesis by recruiting VEGFR1(+) stem cells from bone-marrow microenvironment. *Nat Med*. 2002;8:841–849.
9. Takahashi T, Kalka C, Masuda H, Chen D, Silver M, Kearney M, Magner M, Isner JM, Asahara T. Ischemia- and cytokine-induced mobilization of bone marrow-derived endothelial progenitor cells for neovascularization. *Nat Med*. 1999;5:434–438.
10. Carmeliet P. Angiogenesis in health and disease. *Nat Med*. 2003;9:653–660.
11. Dejana E. Endothelial cell-cell junctions: happy together. *Nat Rev Mol Cell Biol*. 2004;5:261–270.
12. Navarro P, Ruco L, Dejana E. Differential localization of VE- and N-cadherins in human endothelial cells: VE-cadherin competes with N-cadherin for junctional localization. *J Cell Biol*. 1998;140:1475–1484.
13. Corada M, Mariotti M, Thurston G, Smith K, Kunkel R, Brockhaus M, Lampugnani MG, Martin-Padura I, Stoppacciaro A, Ruco L, McDonald DM, Ward PA, Dejana E. Vascular endothelial-cadherin is an important determinant of microvascular integrity in vivo. *Proc Natl Acad Sci U S A*. 1999;96:9815–9820.
14. Liao F, Li Y, O'Connor W, Zanetta L, Bassi R, Santiago A, Overholser J, Hooper A, Mignatti P, Dejana E, Hicklin DJ, Bohlen P, Monoclonal antibody to vascular endothelial-cadherin is a potent inhibitor of angiogenesis, tumor growth, and metastasis. *Cancer Res*. 2000;60:6805–6810.
15. Weis S, Shintani S, Weber A, Kirchmair R, Wood M, Cravens A, McSharry H, Iwakura A, Yoon YS, Himes N, Burstein D, Doukas J, Soll R, Losordo D, Cheresh D. Src blockade stabilizes a Flk/cadherin complex, reducing edema and tissue injury following myocardial infarction. *J Clin Invest*. 2004;113:885–894.
16. Kawamoto S, Niwa H, Tashiro F, Sano S, Kondoh G, Takeda J, Tabayashi K, Miyazaki J. A novel reporter mouse strain that expresses enhanced green fluorescent protein upon Cre-mediated recombination. *FEBS Lett*. 2000;470:263–268.

17. de Bruijn MF, Ma X, Robin C, Ottersbach K, Sanchez MJ, Dzierzak E. Hematopoietic stem cells localize to the endothelial cell layer in the midgestation mouse aorta. *Immunity*. 2002;16:673–683.
18. Tavian M, Coulombel L, Luton D, Clemente HS, Dieterlen-Lievre F, Peault B. Aorta-associated CD34+ hematopoietic cells in the early human embryo. *Blood*. 1996;87:67–72.
19. Loughna S, Sato TN. Angiopoietin and Tie signaling pathways in vascular development. *Matrix Biol*. 2001;20:319–325.
20. Wright DE, Wagers AJ, Gulati AP, Johnson FL, Weissman IL. Physiological migration of hematopoietic stem and progenitor cells. *Science*. 2001;294:1933–1936.
21. Abkowitz JL, Robinson AE, Kale S, Long MW, Chen J. Mobilization of hematopoietic stem cells during homeostasis and after cytokine exposure. *Blood*. 2003;102:1249–1253.
22. Ismail JA, Poppa V, Kemper LE, Scatena M, Giachelli CM, Coffin JD, Murry CE. Immunohistologic labeling of murine endothelium. *Cardiovasc Pathol*. 2003;12:82–90.
23. Allport JR, Muller WA, Luscinskas FW. Monocytes induce reversible focal changes in vascular endothelial cadherin complex during transendothelial migration under flow. *J Cell Biol*. 2000;148:203–216.
24. Su WH, Chen HI, Jen CJ. Differential movements of VE-cadherin and PECAM-1 during transmigration of polymorphonuclear leukocytes through human umbilical vein endothelium. *Blood*. 2002;100:3597–3603.
25. van Buul JD, Voermans C, van der Berg V, Anthony EC, Mul FP, van Wetering S, van der Schoot CE, Hordijk PL. Migration of human hematopoietic progenitor cells across bone marrow endothelium is regulated by vascular endothelial cadherin. *J Immunol*. 2002;168:588–596.
26. Arai F, Hirao A, Ohmura M, Sato H, Matsuoka S, Takubo K, Ito K, Koh GY, Suda T. Tie2/angiopoietin-1 signaling regulates hematopoietic stem cell quiescence in the bone marrow niche. *Cell*. 2004;118:149–161.
27. Nishikawa SI, Nishikawa S, Hirashima M, Matsuyoshi N, Kodama H. Progressive lineage analysis by cell sorting and culture identifies FLK1+VE-cadherin+ cells at a diverging point of endothelial and hemopoietic lineages. *Development*. 1998;125:1747–1757.
28. Wang L, Li L, Shojaei F, Levac K, Cerdan C, Menendez P, Martin T, Rouleau A, Bhatia M. Endothelial and hematopoietic cell fate of human embryonic stem cells originates from primitive endothelium with hemangioblastic properties. *Immunity*. 2004;21:31–41.
29. Taoudi S, Morrison AM, Inoue H, Gribi R, Ure J, Medvinsky A. Progressive divergence of definitive haematopoietic stem cells from the endothelial compartment does not depend on contact with the fetal liver. *Development*. 2005;132:4179–4191.
30. Gory-Faure S, Prandini MH, Pointu H, Roullot V, Pignot-Paintrand I, Vernet M, Huber P. Role of vascular endothelial-cadherin in vascular morphogenesis. *Development*. 1999;126:2093–2102.
31. Kubo H, Alitalo K. The bloody fate of endothelial stem cells. *Genes Dev*. 2003;17:322–329.
32. Ziegelhoeffer T, Fernandez B, Kostin S, Heil M, Voswinckel R, Helisch A, Schaper W. Bone marrow-derived cells do not incorporate into the adult growing vasculature. *Circ Res*. 2004;94:230–238.
33. Sata M, Saiura A, Kunisato A, Tojo A, Okada S, Tokuhisa T, Hirai H, Makuuchi M, Hirata Y, Nagai R. Hematopoietic stem cells differentiate into vascular cells that participate in the pathogenesis of atherosclerosis. *Nat Med*. 2002;8:403–409.
34. Yamashita J, Itoh H, Hirashima M, Ogawa M, Nishikawa S, Yurugi T, Naito M, Nakao K, Nishikawa S. Flk1-positive cells derived from embryonic stem cells serve as vascular progenitors. *Nature*. 2000;408:92–96.
35. Frid MG, Kale VA, Stenmark KR. Mature vascular endothelium can give rise to smooth muscle cells via endothelial-mesenchymal transdifferentiation: in vitro analysis. *Circ Res*. 2002;90:1189–1196.
36. Hattori K, Dias S, Heissig B, Hackett NR, Lyden D, Tateno M, Hicklin DJ, Zhu Z, Witte L, Crystal RG, Moore MA, Rafii S. Vascular endothelial growth factor and angiopoietin-1 stimulate postnatal hematopoiesis by recruitment of vasculogenic and hematopoietic stem cells. *J Exp Med*. 2001;193:1005–1014.

Oxidized-HDL_3 modulates the expression of Cox-2 in human endothelial cells

ELISA CALLEGARI[1*], GIUSEPPE D. NORATA[1,3*], HIROYASU INOUE[2] and ALBERICO L. CATAPANO[1,3]

[1]Department of Pharmacological Sciences, University of Milan, Milan, Italy;
[2]Department of Food and Science and Nutrition, Nara Women's University, Nara, Japan;
[3]Center of the Italian Society for the Study of Atherosclerosis, Bassini Hospital, Cinisello Balsamo, Italy

Received January 9, 2006; Accepted March 13, 2006

Abstract. Modified high density lipoprotein (HDL) has been suggested to modulate endothelial expression of pro-inflammatory genes. Since oxidised HDL (Ox-HDL) has been found in atheromatous plaques and receptors for modified HDL are present on endothelial cells, we investigated the effect of Ox-HDL_3 on the expression of Cox-1 or Cox-2. Ox-HDL_3, increased Cox-2 mRNA and protein expression in endothelial cells while no effect on Cox-1 expression was observed. The intracellular pathways involved in this effect were investigated. The incubation with specific inhibitors of intracellular kinases showed that PI3K is mainly involved in the Ox-HDL_3-dependent Cox-2 induction. Transient transfection experiments suggested that the NF-IL6 response element in the proximal promoter (-327 to 59) is involved in Ox-HDL_3-mediated Cox-2 expression. These data suggest that Ox-HDL induce Cox-2 expression in endothelial cells through a PI3K/NF-IL6-dependent pathway.

Introduction

Numerous clinical and epidemiological studies have demonstrated the inverse relationship between HDL cholesterol and the risk of atherosclerosis (1). Beyond the ability of HDL to remove cholesterol from peripheral tissue, HDL particles have additional beneficial effects on the vascular wall (1-3). HDL can inhibit the chemotaxis of monocytes, the adhesion of leukocytes to the endothelium, the LDL oxidation, the endothelial dysfunction and apoptosis. HDL can also act on the vascular tone through the release of vasorelaxant molecule like NO and prostacyclin (PGI2) (3). We have demonstrated previously that HDL increases the release of PGI2 through the induction of cyclooxygenase 2 (Cox-2) and the coupling with PGI syntase in endothelial cells (4). It has been shown that modification of HDL could affect their function (5,6). Oxidised (Ox-) and modified HDL are present in atherosclerotic plaques (7-9) and human analogues of SR-B1 and LOX-1 have been identified as receptors for modified HDL on endothelial cells. *In vitro*, HDL is readily modified using a variety of oxidants (10), with kinetics similar to that reported for LDL (11). Ox-HDL loses its ability to promote cholesterol efflux (5), to induce nitric oxide release (12) and to modulate the expression of matrix-degrading protease and PAI-1 in endothelial cells (13,14).

In the present study, we have investigated the effect of Ox-HDL_3 on the expression of Cox-2 in endothelial cells and the molecular mechanisms involved.

Materials and methods

Materials. HDL subfraction 3 (d 1.125-1.21 g/ml) was obtained from freshly isolated human plasma by preparative ultracentrifugation and dialyzed in PBS containing 0.01% EDTA (15). HDL_3 (1 mg protein/ml) was oxidized with 20 μM Cu_2SO_4 for 24 h at 37°C, as described (13). The oxidation was blocked by the addition of 40 μM butylated hydroxytoluene (BHT). Under these conditions, we have previously shown that lipoprotein oxidation does not proceed further at 4°C. The LPS content of HDL_3 was measured using an endotoxin kit from Sigma. No contamination was detected (data not shown). Native HDL_3 and Ox-HDL_3 were used within 6 h of preparation.

The MEK inhibitor, U0126 (New England Biolabs, Germany), the p38 MAPK inhibitor SB 203580 (Sigma, Italy), and the PI3K inhibitor Ly 294002 (Alexis, Italy) were used at a final concentration of 10 μmol/l, 0.5 μmol/l and 50 μmol/l, respectively (15). At these concentrations the inhibitors effectively decreased the phosphorylation of the downstream targets (data not shown).

HUVECs were isolated as described (16) and cultured under standard conditions in medium M-199 containing 20% FCS (fetal calf serum), heparin (15 U/ml) and ECGF (endothelial cell growth factor, 20 μg/ml) (Roche, Italy). The cells

Correspondence to: Dr Giuseppe D. Norata, Department of Pharmacological Sciences, University of Milan, Via Balzaretti 9, I-20133 Milan, Italy
E-mail: danilo.norata@unimi.it

*Contributed equally

Key words: high density lipoprotein, Cox-2, endothelial cells

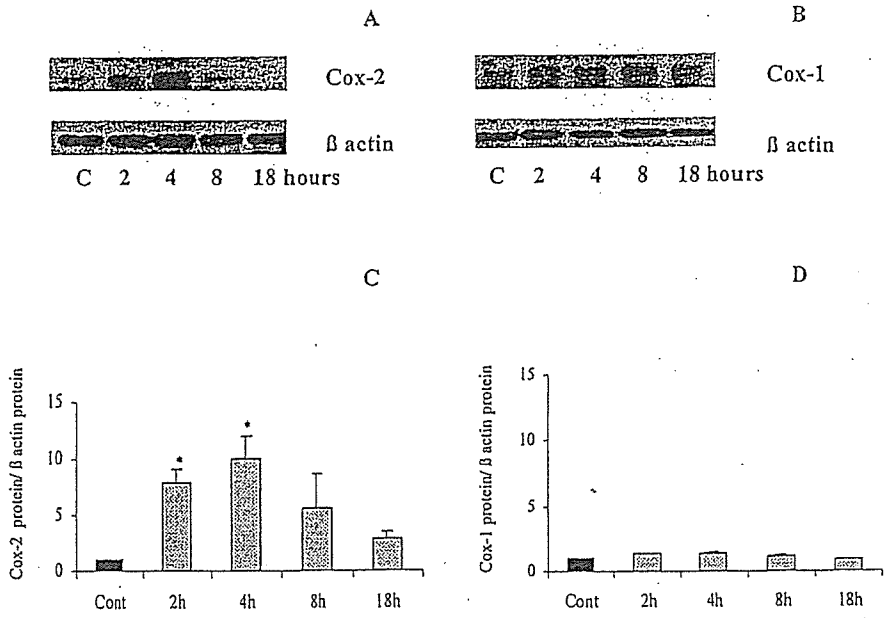

Figure 1. Effect of Ox-HDL_3 on Cox-2 and Cox-1 protein expression in endothelial cells. HUVECs were incubated with Ox-HDL_3 30 μg/ml for 2, 4, 8, 18 h. Cells were lysed and the lysates were analysed by immunoblotting using anti Cox-2 (A) and anti Cox-1 (B). The blot was stripped and reprobed with anti ß-actin to confirm equal expression (A and B). Results from 3 different experiments are presented in (C) and (D) (mean ± SD; *p<0.05 vs control cells).

were used within the 4th passage. Cells were plated in 6-well plates and used after 48 h as subconfluent cultures. In all experiments, cells were preincubated with serum-free medium for 6 h, and then native or Ox-HDL_3 were added for different times. Cells were incubated in the presence or absence of compounds with appropriate chemicals or vehicle additions (DMSO, 0.1% vol/vol).

Real-time quantitative RT-PCR. Total RNA was extracted and underwent reverse transcription as described (4,17). Three μl of cDNA was amplified by real-time quantitative PCR with 1X SYBER Green universal PCR mastermix (Bio-Rad) (4). The specificity of the SYBER Green fluorescence was tested by plotting fluorescence as a function of temperature to generate a melting curve of the amplicon. The melting peaks of the amplicons were as expected (data not shown). The primers used, the amplicon size and the melting temperature have been described previously (4). Each sample was analyzed in duplicate using the IQ™-Cycler (Bio-Rad). The PCR amplification was related to a standard curve ranging from 10^{-11} M to 10^{-14} M.

Immunoblotting. Cox-1 and Cox-2 expression was investigated as described (18). Briefly, cells were plated in 6-well plates and treated with Ox-HDL_3 or native HDL_3 for 5-40 min, then lysed using a Tris-glycine buffer (0.25 M Tris, 0.173 M glycine) containing 3% SDS and 1 mM PMSF (phenylmethylsulfonil fluoride). Aliquots of the samples (15 μg) were diluted in a 2% ß-mercaptoethanol buffer containing glycerol and bromophenol blue and electrophoresed on a 12% SDS-PAGE, then transferred onto a nitrocellulose membrane using a Trans Blot Cell (Hoefer Scientific Instrument, San Francisco, CA) (19). The membrane was saturated at room temperature in PBS containing 3% BSA for 1 h, washed with PBS-T (PBS containing 0.1% Tween-20), then incubated overnight at 4°C with a mixture of primary antibody (1:1000 incubation at room temperature for 1 h for Cox-1 and Cox-2 antibodies;

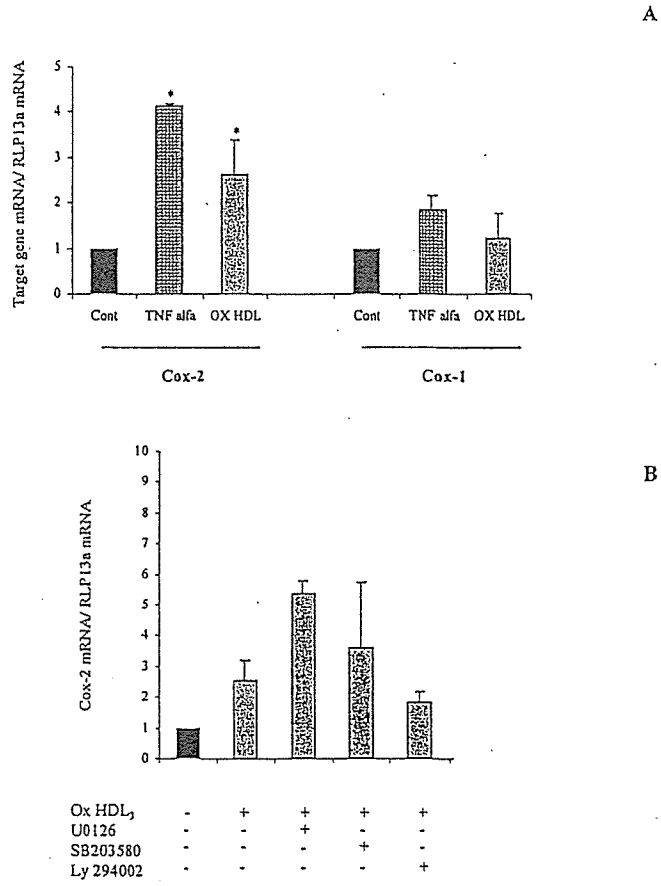

Figure 2. Effects of kinase inhibitors on Ox-HDL_3 induced Cox-2 mRNA expression in endothelial cells. (A) HUVECs were incubated for 2 h for mRNA detection with Ox-HDL_3 (30 μg/ml), or TNF-α (10 ng/ml) used as positive control. Cox-2 and Cox-1 mRNA expression was measured by quantitative real-time PCR and normalised to RLP13a mRNA expression. (B) HUVECs were incubated for 2 h with Ox-HDL_3 (30 μg/ml) alone or in presence of U0126 (10 μM) or SB 203580 (0.5 μM), Ly 294002 (50 μM). Cox-2 mRNA expression was measured by quantitative real-time PCR and normalised to RLP13a mRNA expression. The mean ± SD from 3 different experiments is shown. *p<0.05 vs control cells.

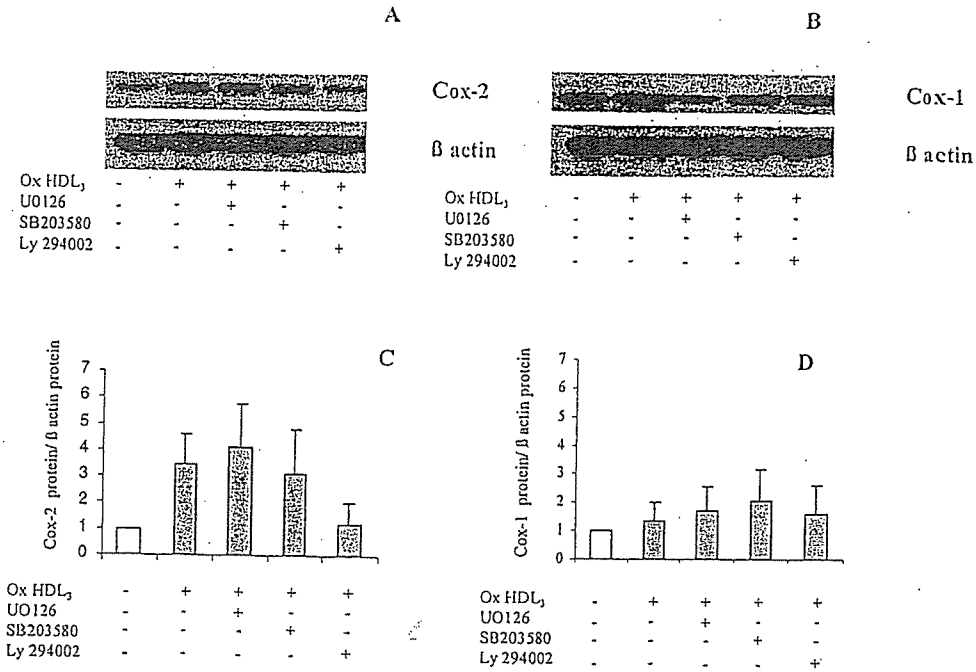

Figure 3. Effects of kinase inhibitors on Ox-HDL_3 induced Cox-2 and Cox-1 protein expression in endothelial cells. HUVECs were incubated for 6 h with Ox-HDL_3 (30 μg/ml) alone or in presence of U0126 (10 μM) or SB 203580 (0.5 μM), Ly 294002 (50 μM) and SH-5 (10 μM). Cells were lysed and the lysates were analysed by immunoblotting using anti Cox-2 (A) and anti Cox-1 (B). The blot was stripped and reprobed with anti ß-actin to confirm equal expression (A and B). Results from 3 different experiments are presented in (C) and (D) (mean ± SD).

1:1000 incubation at room temperature for 1 h for ß-actin antibody) followed by a 1:1000 dilution of peroxidase-conjugated anti-mouse IgG (Sigma) or peroxidase-conjugated anti rabbit IgG (Bio-Rad, Italy). Immunocomplexes were detected by an enhanced chemiluminescence method (ECL, Amersham, Italy), followed by autoradiography and quantified by the Image program (NIH 1.52).

Transfection assay. Transient transfection experiments were first performed using HUVECs and EAhy 926 cells; however, the efficiencies reached were very low with a high degree of cytotoxicity (data not shown). As human Cox-2 promoter regulation is similar in a wide number of cell types we performed transfection experiments in CHO cells, a cell line widely used for studies involving the effects of HDL *in vitro* (4,20). CHO cells were transiently transfected with Cox-2 (nucleotide -327/+59), the NF-κB mutated site (KBM) or the NF-IL6 mutated site (ILM) luciferase reporter vectors using a calcium phosphate precipitation method as described (4). ß-galactosidase activity was assayed as described (14). Luciferase activity was determined and normalized to the ß-gal activity of the cotransfected pSV-ß-galactosidase construct.

Statistical analysis. Data presented in the text and figures are mean ± SD and are representative of 4 different experiments. Statistical analysis was performed by ANOVA with the use of Statsoft Statistica Package.

Results

The experimental set-up was designed to analyse endothelial cell expression of Cox-1 and Cox-2 in the presence of Ox-HDL_3 in relation to basal conditions. The cells were kept in a serum-free medium for 6 h; then HDL_3 (30 μg/ml) or Ox-HDL_3 (30 μg/ml) were added for 4 h. Control cells were incubated for 4 h with the experimental medium containing the same percentage of PBS that was added with the stimulus.

Cox-2 protein was expressed at low levels in unstimulated cells and was strongly induced 2 h after exposure to Ox-HDL_3 (30 μg/ml); the induction was maximal after 4 h and decreased after 8 h (Fig. 1). Cox-2 expression in unstimulated cells remained low at all time points (data not shown). Ox-HDL_3 did not affected Cox-1 protein expression (Fig. 1). Next we examined the effects of Ox-HDL_3 on the Cox-1 and Cox-2 mRNA expression. The cells were kept in a serum-free medium for 6 h; then Ox-HDL_3 (30 μg/ml) or TNF-α (10 ng/ml), used as positive control, were added for 2 h. We observed the induction of Cox-2 mRNA expression by Ox-HDL_3 (30 μg/ml) or TNF-α (10 ng/ml), while no effect was observed on Cox-1 mRNA expression.

To investigate the role of ERK1/2, p38 MAPK and PI3K/Akt pathways in Cox-2 expression induced by Ox-HDL_3, cells were preincubated with the MEK1 inhibitor U0126, the p38 MAPK inhibitor SB 203580 and the PI3K inhibitor Ly 294002 for 1 h; Ox-HDL_3 (30 μg/ml) were then added for 2 and 4 h to evaluate Cox-2 mRNA and protein expression (Figs. 2 and 3). U0126 was unable to block Ox-HDL-induced Cox-2 expression. SB 203580 partially inhibited Ox-HDL-induced Cox-2 expression while Ly 294002 completely abolished Ox-HDL-induced Cox-2 mRNA expression and partially inhibited protein expression. No effect of SB 203580 and Ly 294002 was observed on Cox-1 protein expression.

Next we examined the effects of Ox-HDL on the Cox-2 promoter activity. The human Cox-2 promoter region (-327/+59) contains the NF-κB, the NF-IL6 and the CRE sites

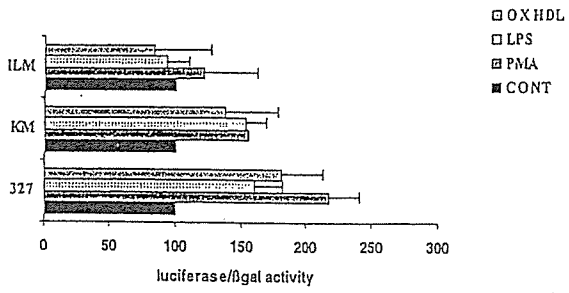

Figure 4. Identification of the regions responsible for Ox-HDL_3-induced promoter activity of the human Cox-2 gene. Following transfection, CHO cells were incubated for 6 h with LPS (1 μg/ml) or PMA (50 ng/ml) both used as positive control, and with Ox-HDL_3 (30 μg/ml). The results are presented as relative luciferase activity normalized to ß-galactosidase activity. Each experiment was carried out in triplicate.

(4,18). Transient transfection assay showed that Ox-HDL induced promoter activity by 199±27% (Fig. 4). PMA, used as positive control, induced promoter activity by 218±35% while LPS induced promoter activity by 160±29% (Fig. 4). Upon incubation with Ox-HDL, the promoter activity of the construct carrying the mutation at the NF-κB site was 140±48%, that of the construct carrying the mutation at the NF-IL6 site was 71±26% (Fig. 4). Upon incubation with PMA the promoter activity of the construct carrying the mutation at the NF-κB site was 155±14%, that of the construct carrying the mutation at the NF-IL6 site was 93±13% (Fig. 4); finally upon incubation with LPS the promoter activity of the construct carrying the mutation at the NF-κB site was 156±24%, that of the construct carrying the mutation at the NF-IL6 site was 83±32% (Fig. 4), thus suggesting a major role of the NF-IL6 site on the effect observed.

Discussion

Several lines of evidence have accumulated indicating that oxidative modification of HDL can occur *in vivo* (10,11,21,22). Furthermore, investigations using the Ox-HDL-specific 9F5-3a antibody have indicated the presence of Ox-HDL in the intima of atheromatous plaques in the human abdominal aorta located specifically in aortic endothelial cells (7), and in sera from patients with chronic renal failure (23). In addition, oxidative modification of HDL not only attenuates its beneficial properties, such as stimulation of cholesterol efflux from foam cells (21), endothelium-dependent vaso-reactivity (24) and anti-oxidative activity (10), but also generates a pro-atherogenic species that inhibits nitric oxide synthesis in endothelial cells (25) and induces production of reactive oxygen species and apoptosis via NF-κB activation (26). Several genes involved in the inflammatory response observed during atherogenesis are modulated through the activation of the NF-κB pathway, including Cox-2 (27).

Here we demonstrated that Ox-HDL could play an harmful role by inducing Cox-2 expression. This effect was specific for Cox-2 as no effect on Cox-1 induction was observed and is dependent upon the activation of intracellular signalling pathways regulating the transcription machinery. We have previously shown that Ox-HDL could modulate PAI-1 expression through the activation of the p38 MAPK pathway promoting RNA stabilization (14). For Ox-HDL-induced Cox-2 expression the p38 MAPK or the ERK1/2 pathway seems to play a minor role, while the activation of the PI3K pathway is fundamental for Ox-HDL-dependent Cox-2 expression in agreement with previous observation with a different experimental setting (28).

To determine the specific transcription factor that is involved in the Ox-HDL mediated Cox-2 expression, we examined the effects of Ox-HDL on the luciferase activity of plasmids containing the Cox-2 promoter defective in the NF-κB or the NF-IL6 binding site (4,18).

Our data clearly demonstrated that the NF-IL6 site is implicated is the response observed. NF-IL6 is a member of the C/EBP family of transcription factors and is involved in inducing several acute-phase protein genes in response to immune and inflammatory stimulation. NF-IL6 also plays a mayor role in inducing the expression of Cox-2 by cytokines and endotoxin (29) thus suggesting that Cox-2 induction by Ox-HDL via NF-IL6 could depend on a pro-inflammatory activated endothelium.

What are the physiological implication(s) of our data? The possibility that Cox-2 plays a harmful role by catalysing the biosynthesis of pro-inflammatory prostanoids has been suggested. Cox-2 immunostaining has been observed in macrophages/foam cells, intimal and medial smooth muscle cells and endothelial cells in atherosclerotic arteries, whereas normal arteries contained no Cox-2 protein (27). Similarly, Schonbeck *et al* (30) found expression of both Cox-1 and Cox-2 by endothelial cells, smooth muscle cells and macrophages in atherosclerotic arteries, while normal arteries only expressed Cox-1. Furthermore, Cox-2 and prostaglandin synthase E colocalize in symptomatic lesions and are possibly involved in metalloprotease activation via PGE_2 production (31) suggesting a role for PGE_2 in plaques instability.

On the other hand, Cox-2 might play an atheroprotective role (27). *In vitro* laminar shear stress upregulates Cox-2 mRNA and protein in HUVEC, turbulent shear stress does not have this effect (32). Prostacyclin is a potent vasodilator, inhibits platelet aggregation and blocks leukocyte adhesion and activation (33). It is therefore possible that Cox-2 induced in endothelial cells at lesion-protected areas catalyses the formation of the anti-atherogenic molecule prostacyclin. These finding suggest the possibility that Cox-2 induction alone is not enough to drive prostaglandin production toward a pro-atherogenic or anti-atherogenic profile, but the prostanoids produced account for this effect. Future studies are thus warranted to identify the prostanoid profile induced by Ox-HDL in the endothelium.

In summary, we have shown that Ox-HDL induces Cox-2 expression in human endothelial cells through a PI3K, NF-IL6-dependent pathway, suggesting a new mechanism by which Ox-HDL could modulate the inflammatory response in the arterial wall.

Acknowledgements

This work was supported by grants from FIRB (2001-RBNE01HLAK_006), COFIN 2004 (2004065985_006 and 2004069574_003), CIRC (Consorzio Interuniversitario Ricerca Cardiovascolare) and SISA Lombardia (Società Italiana Studio Aterosclerosi).